
# Long-range Unmanned New Artemis Rover Electric Mining Unit (LUNAR EMU)

University of Colorado, Colorado Springs

University of New South Wales

| Name | Role | University | Academic Background |
|---|---|---|---|
| Tyler Tryon | Team Lead | UCCS | Mechanical Engineering, UGRD |
| Dawson Burch | Rover Body | UCCS | Mechanical Engineering, UGRD |
| Peter Johnson | Power Systems | UNSW | Aerospace Engineering, UGRD |
| Phoebe Loughhead | NAV / COMM | UNSW | Aerospace Engineering, UGRD |
| Dr. Lynnane E. George | Faculty Advisor | UCCS | Mechanical Engineering, PROF. |

# Abstract

The UCCS NASA RASC-AL senior design team worked in collaboration with the University of New South Wales (UNSW) from Sydney, Australia, to create LUNAR EMU, a dual rover architecture created to find and analyze substances in the south lunar craters to help bring a sustained human presence to the NASA Artemis missions. Conforming to NASA and self created guidelines and requirements, LUNAR EMU can travel 464.8km on hydrogen fuel cell technology with an operating lifetime cost of $212.6 million, ready to launch by August of 2032 due to its high technical readiness level (TRL). If it travelled at the same speed of an average Martian rover, it can travel continuously for 56 years. It has an array of scientific equipment from cameras to mass spectrometery to identify the materials of interest, and the dual rover architecture allows it to explore two areas of interest at once making it an efficient exploration vehicle.

# LUNAR EMU Team

**Team Lead**

Tyler Tryon

UCCS Mechanical Engineering senior, minoring in Aerospace Engineering. Working as a systems engineer intern contractor for OPIR MBSE and V&V analysis, civilian scientist of the NASA DEB Initiative, and TA for UCCS.

**Prototype and Rover Body Lead**

Dawson Burch

UCCS Mechanical Engineering senior, minoring in Aerospace Engineering. Competed in the 2021-2022 AIAA Design Build Fly competition working on the propulsion subsystem, and a TA for UCCS.

**Power Systems Lead**

Peter Johnson

UNSW 5th year Aerospace Engineering student completing an undergraduate Honours thesis in 2024 on "Hydrogen Powertrain Design for Lunar Vehicles". Competed in the 2022 and 2023 Over the Dusty Moon Challenge, 2023 WMC Hackathon and ELO2 Regolith Acquisition Challenge.

**Navigation and Communications Lead**

Phoebe Loughhead

UNSW 6th year Engineering/Science student majoring in Aerospace Engineering and Physics. Currently participating in the 2023-24 AIAA Design Build Fly competition as Project Lead for the UNSW team. Previously Aerodynamics Lead for the 2022-23 competition.

**Faculty Advisor**

Dr. Lynnane E. George

Mechanical and Aerospace Engineering senior instructor at UCCS, teaching electronics, space systems, and robotics, avid STEM Community outreach volunteer. Served in the US Air Force, earning the rank of Lieutenant Colonel, working mostly on rockets and space systems.

# Contents

# List of Figures

# List of Figures

# 1 Introduction

The Long-range Unmanned New Artemis Rover Electric Mining Unit (LUNAR EMU) is a TRL-3 dual rover architecture, powered by hydrogen fuel cells, aimed to efficiently and effectively find ice, Helium-3 (He3) for fusion reactors, and other rare minerals and resources on the lunar south pole, assisting the Artemis Missions bringing a sustained human presence to the surface of the moon [1, 2, 3]. The rover design takes inspiration from aspects of the upcoming NASA VIPER mission but integrates flight proven materials and pre-existing TRL-6/7 technology from early space flight during the Apollo and Space Shuttle eras, making it feasible for operation by 2033. Although utilising many proven, existing technologies, LUNAR EMU features a revolutionary system design which would allow it to not only 'survive the night', but operate throughout it by travelling up to 464.8 km, equivalent to 56 years at average Martian rover pace between Perseverance and Curiosity, in the near absolute temperatures of 25-30 K within the permanently shadowed regions (PSR) of the moon [4, 5]. The overall system architecture consists of a large primary rover, 'EMU', containing all scientific equipment and hydrogen fuel cell powertrain technology which serves as a mobile platform for operations. The primary EMU rover is complimented by a smaller supplementary rover, Little - EMU or 'LEMU', utilized for scouting terrain and collecting samples from areas of interest (AOIs). The dual rover architecture optimizes sample collection by targeting two different AOIs at the same time. Although the rovers will be well suited to deal with any lunar terrain, there are three primary target craters which may possess materials critical for a lunar habitat: Shackleton Crater, Amundsen Crater, and the Shoemaker Crater, as the regolith in these regions may contain a 5% water mass concentration [6, 7, 8, 9, 10, 11].

# 2 Design Architecture

Taking inspiration from the Apollo Lunar Roving Vehicle (LRV), both rovers will be predominantly manufactured using aluminum alloy Al2219, a lightweight alloy with inherent electrical insulative properties to protect the rover from the regolith's static charge [12]. Al2219, most critically, is capable of withstanding the extreme temperature conditions of the lunar surface, as low as 20 K, making it a reliable material selection for both EMU and LEMU as it maintain its strength as the temperature decreases [13, 14, 15]. All systems will be encased within an Al2219 shell, similar to NASA VIPER, as a dust mitigation measure to support system longevity and mission success [16]. Later iterations of LUNAR EMU will utilize a new material aluminum alloy, Al2195, due to its 5% decrease in density [14, 17, 18]. It is not being implemented in the first LUNAR EMU design, however, due to its largely understudied electrical resistivity and the relative novelty of the alloy.

Figure 1 illustrates the mission flow chart following the launch. The launch vehicle selected for the mission is SpaceX's Falcon Heavy, which will inject LUNAR EMU into a Low Earth Orbit (LEO) parking orbit. From LEO, system checks, including but not limited to camera feeds, successful downlink to Earth over the Deep Space Network (DSN), and star mapping will be performed to monitor for nominal mission performance. If these fail and troubleshooting and problem solving cannot fix any detected issues, the rover will be decommissioned and deorbited on a trajectory for Point Nemo. If all checks pass and all systems are showing nominal performance, LUNAR EMU will enter a trans-lunar orbit via a retrograde orbit, to enter a highly elliptical, high inclination orbit (HEO) using the upper stage of Falcon 9. Initiating an orbital capture burn around the lunar south pole will bring LUNAR EMU into a polar lunar parking orbit. LUNAR EMU will utilize an analytical approach for a LEO to Lunar-transfer orbit to ensure mission success and reduce fuel requirements [19]. The landing descent phase of the mission will begin with the sky crane, a technology which has demonstrated it would be capable of delivering the 946.67 kg dual rover payload to the lunar surface [20, 21]. The PEM engine ignition will occur at an altitude of 1.8 km, at which point the rover will unfold from its payload configuration in preparation for landing. The Skycrane will detach from EMU at an altitude of 20 m and perform the 'Skycrane maneuver' where the Skycrane will perform its own uncontrolled landing away from LUNAR EMU to avoid causing any ballistic damage [22]. After touchdown, the rovers will undertake further system checks, verifying

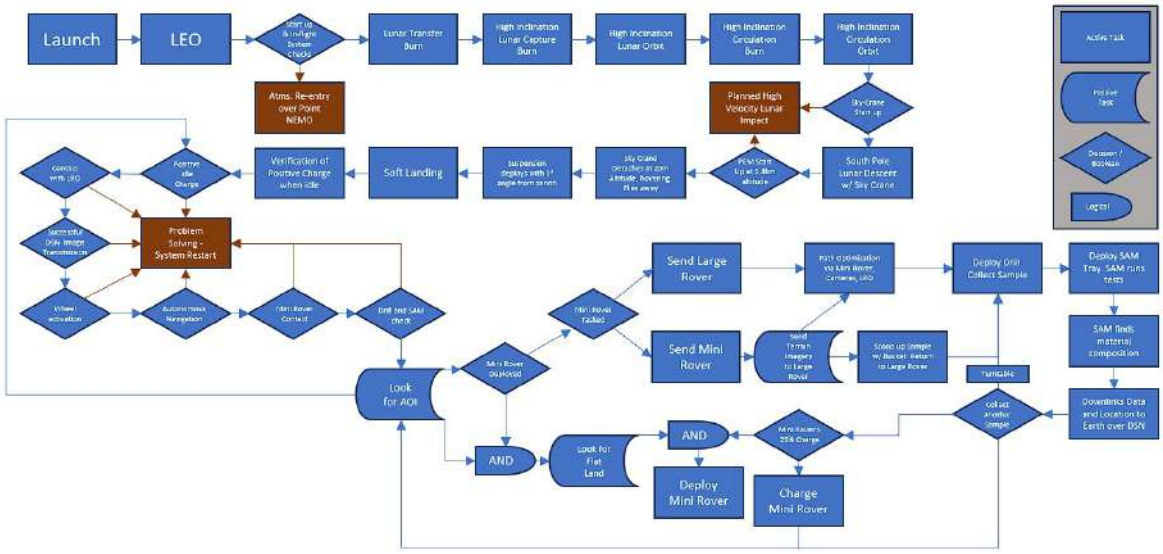


Figure 1: Mission Flow Chart

everything is operating nominally. Once these system checks pass, EMU and LEMU will begin their mission profile searching for valuable resources.

## 2.1 Power

Three main power generation technologies, used previously in spaceflight, were considered for the LUNAR EMU mission: Photoelectric cells, Radioisotope Thermoelectric Generator (RTG), and Hydrogen Fuel Cells. The craters targeted in the mission are PSRs as sunlight never reaches the crater beds due to the natural topography of the Lunar south pole. Therefore, photoelectric cells were immediately omitted. Although RTGs are popular on current operational Martian rovers such as Curiosity and Perseverance [23, 24], their high manufacturing cost made them less desirable than hydrogen fuel cells [25]. Many different types of hydrogen fuel cells exist, but a Proton-Exchange Membrane (PEM) Fuel Cell was selected due to its simplicity and low weight [26]. In a PEM fuel cell, H2 and O2 pass into an anode and cathode respectively, before entering a PEM layer. This interaction causes the protons and electrons to separate. The electrons are forced through an external circuit, generating the power required for the LUNAR EMU mission. Appendix C shows the schematic of an individual PEM Fuel Cell which will be used on EMU. LUNAR EMU will feature a stack of 200 cells with a density of 0.9 A/cm$^3$, producing 130 V of usable power. This configuration was optimized from data plotted in Appendix D.

Hydrogen fuel cells are capable of operating in extremely low temperatures, however, to operate in the temperatures LUNAR EMU will experience, dropping below 50 K, a special Platinum catalyst will be required [27]. This inherently makes the system more susceptible to carbon monoxide poisoning, so all fuel loaded into EMU will need to be carefully processed if it is derived from hydrocarbons. This will ensure the powertrain can operate nominally throughout the duration of the LUNAR EMU mission. By storing the fuel in the cryogenic conditions of 50.5 bar and 55 K, just 5 K above the average lunar surface temperatures, the rover will be capable of travelling a distance of 174.4 km on a fuel reserve consisting of 126.1 L of LH2 and 21.0 L of LO2. In total, this is the equivalent of 1.01 GJ of energy at maximum fuel cell efficiency [28]. Using the average Martian rover speed of 7.9 km/yr, this allows a maximum lifespan of over 56 years, successfully fulfilling LUNAR EMU's role as a large scale lunar crater prospector [29, 30, 5].

High density LiPo batteries will be implemented as power reserve banks for both rovers. These will provide

extra charge when required, and ensure the rover is operational during instances when the PEM fuel cell is inactive, such as during launch and orbit. Utilizing Ultra High Energy Cells, the batteries can output 220 Wh/kg for 200 cycles [31]. Future iterations of the LUNAR EMU mission will utilize advancements emerging solid-state batteries, such as those being researched under NASA's Solid-state Architecture Batteries for Enhanced Rechargeability and Safety (SABERS) program. These batteries offer higher energy densities compared to traditional lithium-ion batteries, producing 500 Wh/kg for near unlimited cycles [32, 33]. A considerable benefit of implementing SABERS is that the batteries can be stacked more compactly, saving between 20-30% in mass savings by removing excess material [32]. This concept is still undergoing research and development, however, if successful it would be suitable for integration into LUNAR EMU once it has satisfied TRL-6/7 requirements.

## 2.2 Thermal Management

Although the rover is designed to operate in near absolute zero conditions, the PEM fuel cells will be producing a considerable amount of thermal energy. LUNAR EMU will utilize a passive heat exchange system through copper heat sinks which will radiate heat from the powertrain into space, similar to satellite Passive Radiative Coolers (PRCs), capable of transferring over 20 mW of heat at 85 K [34]. LUNAR EMU will experience average low temperatures of 50 K, which will reduce the efficiency of the PRC. To mitigate this problem, a larger heat sink than what is standard on Earth orbiting satellites was incorporated into the LUNAR EMU design, lining the inner walls of EMU to maximize the radiating surface area. This will optimize its radiative capacity, maximizing the heat transfer away from the rover. Further thermal management could be implemented by adding pressurized refrigerant within the PRC, increasing the heat transfer to 200 mW [35]. Despite the added benefits, a liquid refrigerant thermal management system would increase the rover's complexity and overall mass, and was omitted on the preliminary design of LUNAR EMU. The heat sinks are pointed away from the cameras to reduce any thermal noise which could disrupt the highly sensitive infrared and night vision cameras [36].

## 2.3 Propulsion

Two wheel designs were considered to maximize traction in uncompacted regolith: non-pneumatic and paddle wheels. Non-pneumatic wheels naturally deform under load to maximize the ground contact surface area, yielding high traction capabilities without slip. These wheels, although proven to work on the lunar surface with the LRV using a non-pneumatic wire-mesh variant, proved to fail under long duration JPL testing [37, 38, 39, 40]. The wheel design, however, reduces energy loss on impact with an obstacle and displaces less regolith than pneumatic wheels - leading to more traction, without encountering more resistance [41, 38]. The paddle wheel, also called a lugged wheel, was implemented to go over the expected rough terrain and obstacles at the expense of the highest and most oscillatory power requirement over other wheel designs, shown by JPL and CalTech research in Appendix F.1 [42]. Despite the large and uneven power requirements, the sinkage of the lugged wheel was the highest, followed by the non-pneumatic wire-mesh wheel, shown in Appendix F.4 [43]. The increased sinkage into the soil allows more surface area and thus greater traction. The upcoming NASA VIPER plans on utilizing this wheel type in order to traverse over large obstacles with high durability [44]. EMU utilizes large 0.5 m diameter hybrid pseudo-non-pneumatic double-tire lugged wheels, allowing for 3cm of repetitive elastic deformation, shown in Appendix K.2.

The rovers will utilize a torsion bar suspension system due to their flight proven effectiveness on the Apollo LRV [13]. A brushless DC motor will be mounted on each of the torsional spring damped torsional bars allowing all six wheels to be controlled independently. Unlike Martian rovers, which maneuver by rotating the front and rear wheels, EMU and LEMU will maneuver similar to many modern military tanks by varying the rotational speed of the wheels on each side. This design consideration was made to mitigate the number of moving parts exposed to the static regolith, decreasing the risk of damage to mission critical components and complexity of the wheel assembly. Electronically actuated, spring loaded 0.32 m torsional bars are utilized for the suspension system, allowing the wheel height of each wheel to be controlled independently. The torsional springs will be

loaded by high torque 12 V worm geared DC motors, augmenting the extent each torsional bar can deflect and providing additional suspension to any natural deflections of the torsional bars. This design feature allows for 0.57 m of suspension travel which can be altered as required during the mission, along with an additional 30 mm of dampening due to the wheel and torsional bar deformation. LEMU utilizes scaled down wheels with a diameter 0.25 m and torsional bars with 0.1 m of suspension travel.

## 2.4 Scientific Equipment

### 2.4.1 EMU

EMU will contain the majority of the scientific equipment used for the detection and verification of materials on the lunar surface. This will largely be comprised of four distinct cameras of different wavelengths, namely, visible light, near-infrared (NIR), short-wave-infrared (SWIR), and night vision cameras. This camera combination covers the full electromagnetic spectrum that ice and other targeted resources will reflect and emit in the low light conditions of the lunar south pole. By matching the detected wavelength signature of a target, with the known reflection curves of resources, EMU will be capable of identifying resources at range. A 1 m long auger drill will be used to acquire samples deep within the regolith, similar to NASA VIPER, by a 1.1 m telescoping arm [45]. The drill will be attached to an offset 0.5 m turntable to allow for the acquisition of multiple local samples and avoid damaging the drill on obstacles, without repositioning the rover. This design was chosen to acquire multiple local samples in a more energy efficient manner, extending the overall life of the mission. Once a sample is collected by the auger drill, the drill will be retraced by the telescoping probe and deposited into a sample tray. The tray will be translated by a rack and pinion system into a modified SAM unit. Although the SAM unit detects biological samples on Martian rovers, it features all the necessary scientific instruments to determine the composition of the lunar regolith, featuring a gas chromatographer, mass spectrometer, tunable laser spectrometer, sample manipulation system, and a 1,000 °C furnace [46, 47]. Appendix G depicts the reflection curves the LUNAR EMU mission will be targeting, as provided by the European Space Agency (ESA) [48].

When an AOI is identified by EMU, it will begin sample collection and analysis procedures. These are undertaken by positioning the rover over the target and deploying the central drill for a pecking drill operation, allowing the drill to acquire layered samples which, when analyzed, will allow the rover to develop a gradient map of the target area. Composition data from the SAM unit, and location data will be sent to Earth over the DSN and Lunar Reconnaissance Orbiter (LRO) for data recording and further analysis [49]. EMU will also be equipped with 12 seismometers, which will be dropped from the underbelly of EMU, throughout the mission and used to assist in the understanding and identification of lunar mineral deposits through composition analysis [50]. This combination of resource detection equipment will give the LUNAR EMU an unprecedented capability to accurately detect and locate resources, fulfilling its role of assisting the Artemis Missions.

### 2.4.2 LEMU

LEMU will feature a night vision and NIR camera, allowing it to detect certain reflective materials, including ice; however, its primary objective is to map terrain. This will allow LEMU to compile data used to develop path optimization for EMU which will undertake the bulk of the resource analysis operation. This is to prevent EMU taking a path in an unmapped area over challenging or potentially harmful obstacles which would be capable of damaging the rover or resulting in unnecessarily expending power and time. LEMU will feature a 4.525 L bucket capable of scooping 0.16 m into the surface layer regolith which will be actuated by a high torque DC worm gear motor, and be deposited into EMU's SAM unit. The combined operation of EMU and LEMU will allow the LUNAR EMU mission to perform multiple operations simultaneously, improving the efficiency and effectiveness of the mission hardware in all aspects.

## 2.5 Communication

EMU will feature a two degrees of freedom, 0.26 m parabolic antenna dish capable of transmitting and receiving over S and X band communications from 2-4 Ghz and 8-12 Ghz respectively, the same frequencies of DSN [51, 52]. The antenna can either transmit directly to Earth based ground stations or relay data via lunar orbiters, such as the LRO or other lunar orbiters launching in the coming decade [49]. LEMU will also communicate over the S and X band wavelengths; however, utilise a much smaller, 0.1 m antenna as it primarily communicate only to EMU. Connection to orbiting satellites also guarantees rover communication to each other despite possible electromagnetic interface around the horizon and terrain obstacles [53].

## 2.6 Navigation

Through star mapping technology from the four onboard cameras, EMU will be able to determine it's rough position and orientation on the lunar surface with an accuracy of 15-21 m [54, 55]. If necessary, a more accurate approximation of EMU's location can be determined utilising the ephemeris data from lunar orbiters, and the orientation of the antenna dish [49]. As more satellites are placed into orbit around the Moon, this precision positioning technology will be able to increase in accuracy, similar to Earth-based GPS technology. LEMU will be able to scout for dangerous terrain, obstacles and AOI's to generate a detailed, localised terrain map. EMU will use the collated data to find the optimal path to any identified AOI. Machine Learning (ML) and Artificial Intelligence (AI) will be used to map terrain topology and determine path optimization, similar to current Perseverance rover [56].

## 2.7 Dust Mitigation

Dust in the PSRs of the moon is believed to be more difficult to remove than in the sun due to the cold temperatures, prompting LUNAR EMU to utilize two different countermeasures [53]. Al2219 is being used as the primary material for the rover body as its electrical insulative properties will reduce the extent to which the static regolith can attach itself to the rover components. In addition, active dust mitigation will be employed using 23 L of LN2 stored onboard the rover which will have ejection ports located around all critical and vulnerable components, controlled by an electronically actuated valves [57]. These locations include the four cameras, motors, wheels, torsional bars, drill, SAM unit and tray, electrical components, and the LEMU charging port.

## 2.8 Systems Engineering

Figure 2 depicts an in-depth overview of how all sub systems within EMU interact with each other with technical and mechanical specifications included. The operations and interactions of all components depicted complies with the mission requirements outlined by the flow chart in Figure 1 to ensure the success of the LUNAR EMU mission. It should be noted that Figure 2 is not to scale, as all motors are 0.7 Nm 12 V high torque motors with 12 rpm technical specifications. EMU operates by feeding $H_2$ and $O_2$ into the PEM fuel cell stack, as stated in section 2.1. All fuel is passed through a one-way valve to prevent back flow. The exhaust, composed of $H_2O$, is stored in an 11.3 L holding tank to prevent false AOI identifications and sample contamination. Only after an area is thoroughly examined will the exhaust $H_2O$ be expelled from the rover through a heated pipe. The resultant power is fed into a power diverter which will transform the power output to a constant voltage and send it the the various power intensive components. All main electronic signals pass through an "Amplifier/Filter". Depending on each components requirements, the output power will be amplified from the power diverter using a transformer diode setup. This is particularly useful for the 12 V required to run motors. Alternatively, the output power will be filtered using a gain-filter for all camera and imagery components to reduce noise. The Main Processor is the primary computer onboard EMU and will manage all computational functions and operations such as fuel valves, wheel and suspension motors, communication data, autonomous navigation, and dust purging actions detailed in Sections 2.3, 2.5, 2.6 and 2.7 respectively. Heat will be captured

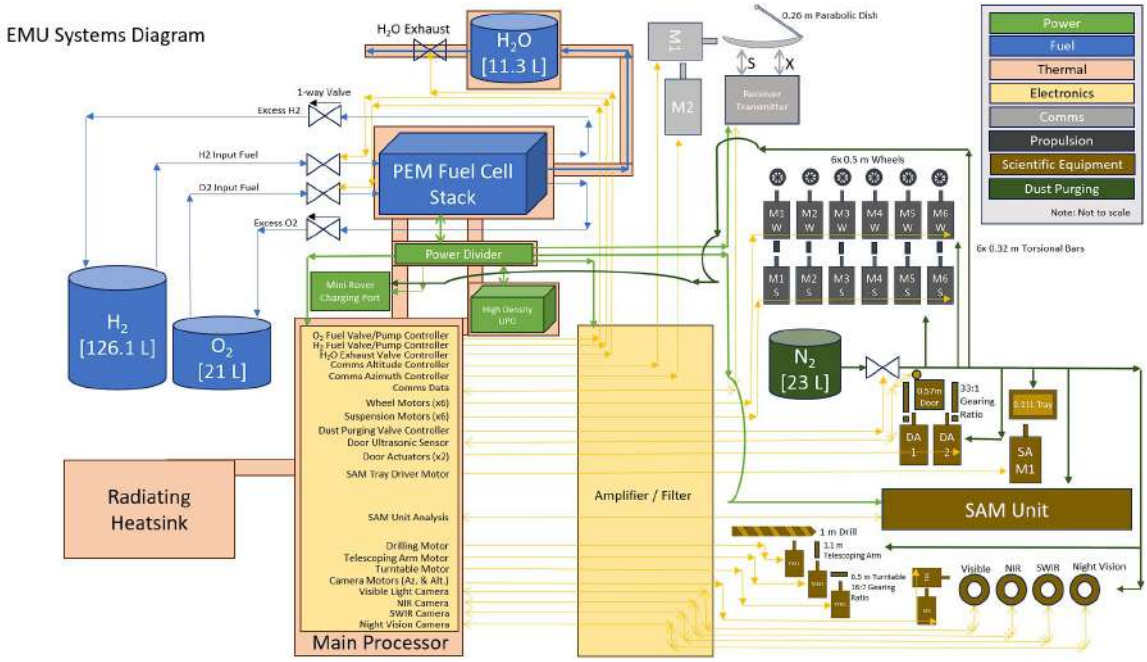


Figure 2: EMU System Diagram

and transmitted through conduction using copper heat sinks around the PEM fuel cell stack, exhaust, processor and battery, with excess being radiated away from the rover body and into space as outlined in Section 2.2. The scientific equipment, outlined in Section 2.4.2, includes the LEMU stowing bay. This section of EMU contains two motors on each side which will move the 0.57 m bay door with a 33:1 gear ratio, as derived from Appendix H. The SAM tray rack and pinon system also moves via a motor. The drilling subsystem consists of a motor with a 16:7 gearing ratio which rotates the turntable drill configuration, on which a 1.1 m telescoping arm is mounted, followed by the drilling motor for the 1 m drill.

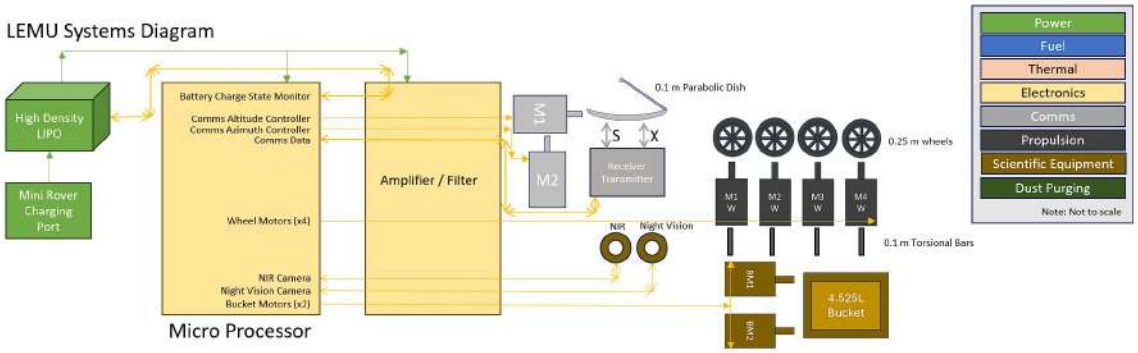


Figure 3: LEMU System Diagram

LEMU takes on a very similar but simplified system diagram, shown in Figure 3. A key difference is powered by high density LiPo batteries instead of a regenerative power source. This is to reduce the complexity, weight and size of the rover, improving its mobility and allowing it to fulfill its complimentary role to EMU. LEMU carries less scientific equipment onboard and therefore requires less processing power to sustain nominal operations. The primary onboard scientific systems include the sample retrieval bucket and two cameras for AOI detection and navigation as described in Section 2.4.1. The integration and interaction of all other parallel systems illustrated in Figure 3 behave similarly to those discussed previously for EMU. Figure 4 shows an annotated

exploded view of all subsystems shown in Figures 2 and 3 for EMU and LEMU respectively. Appendix I shows photo realist realistic renders of EMU and LEMU.

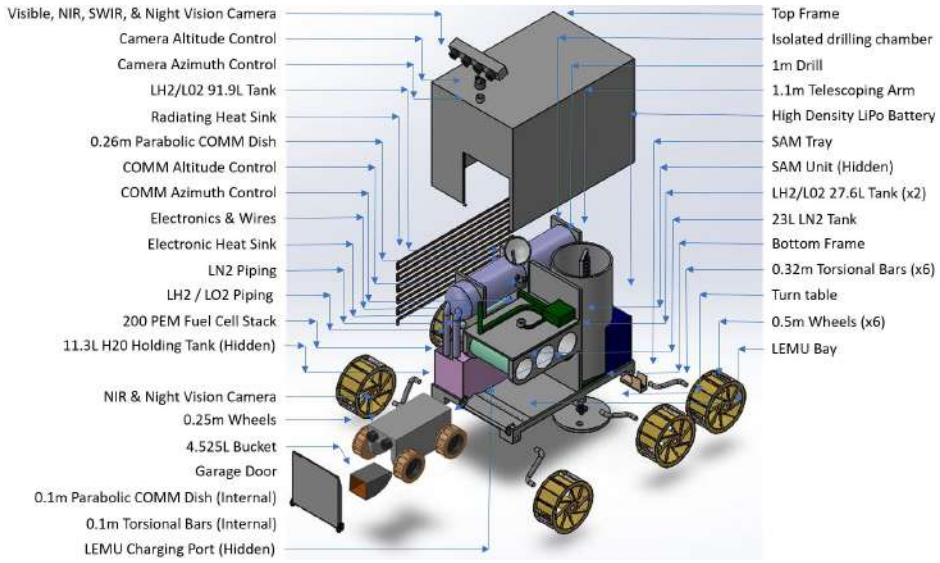


Figure 4: Annotated Exploded View of Subsystems on EMU and LEMU

## 2.9 Capabilities

### 2.9.1 Power

For EMU, the highest load conditions would occur if all six wheels were operating at full speed, the LEMU stowage bay door was closing, LEMU is charging, and all cameras are operational. This scenario outlines when maximum power would be required as all drilling operations would occur when the rover is stationary. If the PEM Fuel Cell stack is behaving nominally, a total of 120 V would be split across the ten separate motors in use. A further 10 V will be delegated to run the cameras, main processor, SAM unit if it is in use, and recharge LEMU, overall resulting in a net negative gain in energy draining from the LiPo Battery. The stowage bay door is designed to take approximately 60 seconds to close during this time, however, once closed, a total of 34 V will be enough to power the SAM unit, electronics, and recharge LEMU and EMU batteries.

### 2.9.2 Environmental Conditions

A key aspect of LUNAR EMU is its ability to travel up a lunar crater wall if its mission is updated and it is required to change locations. This requirement meant it needed to be capable of traversing slopes up to 45° in the loose regolith and low gravity conditions [58]. Using the adjustable suspension, the rover can withstand the following conditions before reaching terminal instability: 51.0° ascending, 54.4° descending, and 56.9° roll in either direction. By design, the center of mass is below all LO2, LH2, and LN2 fuel tanks; as the mission progresses and fuel is expended, the center of mass will drop and move closer to the base of the rover, improving its performance characteristics over all terrain. An additional 10-15° of handling and directional performance can be gained by appropriately adjusting the suspension height of each wheel, making it more susceptible to tipping if it encounters any unexpected obstacle. Overall, this highlights EMU's superlative capabilities at managing all expected environmental conditions.

### 2.9.3 Size and Mass

EMU features a compact footprint of only 1.6 m x 2 m, with a variable height ranging from 1.16 m to 1.73 m depending on the controlled resting angle of the torsion bar suspension. The full payload mass, which is

comprised of both rovers, is 946.67 kg, comparable to the mass of the Perseverance Rover [59]. A considerable portion of this mass is attributed to the Al2219 shell which is used to protect the rover from in-transit radiation and statically charged lunar regolith. Weight could be dropped even further by designing the rover fairing closer to 4 mm in thickness, similiar to SpaceX's Starship [60].

### 2.9.4 Verification and Validation

By cross-checking with all items listed and adhering to the test requirements outlined in Appendix J.1, LUNAR EMU was scrutinised to determine the feasibility of the design. Research, analytical testing, and detailed design inspection was used to determine the boolean status of each requirement on a strict "Pass/Fail" grading. The initial rover design was able to pass all but two requirements, with the two fail items being related to cost and weight. These failed due to the lack of experience in the exoplanetary research field. The full detailed results can be seen in Appendix J.2. FEA was utilized to test mission critical components of the rover, including the suspension, chassis, and fuel tanks. In these analyses all critical components were exposed to simulated operation conditions and all designs were refined to achieve the desired performance capabilities of the rover. The results of these simulations are shown in Appendix K. All desired structural performance parameters have been satisfied through the FEA analyses, however, further physical prototype testing should be employed to validate the results of the FEA simulations.

## 3 Cost and Schedule

The projected cost for the LUNAR EMU rovers production is $31.4 million. This figure is based heavily on cost estimations from the NASA Martian Curiosity rover. Including launch and operational costs, the rover has a complete lifespan cost of $212.6 million. Although this is a considerably large cost figure, the production cost is only 10% of the Curiosity rover and 49% of the comparable NASA VIPER lifetime cost [61, 62, 63]. Cost justifications can be seen in Appendix L. The majority of the manufacturing costs are attributed to the SAM and Skycrane which were both overestimated to be 10% of the Curiosity Rover's total cost, equating to $31.2 million each. This overestimation accounts for production and manufacturing costs, as well as costs attributed to sourcing high quality sub components for the rover systems which can withstand the extreme temperature differentials present across the lunar surface.

Launch costs account for the largest partition of the cost breakdown for the LUNAR EMU mission, which can be reduced by sharing payload capacity with either multiple LUNAR EMUs or other lunar-bound projects. The EMU rover's compact size of 1.6 m x 1.16 m x 2 m could comfortably be contained within the payload bay of SpaceX's Falcon Heavy [64].

Figure 5 depicts the estimated timeline from receiving funding at the beginning of 2025 to producing fully operational rovers on the lunar surface by February of 2033. This schedule breakdown includes a 6 month window for payload and launch vehicle stacking and integration. This overcompensation is designed to act as a buffer in the event that project progression is restricted and key milestone dates are missed. The current LUNAR EMU design is at a TRL-3, with aspects in TRL-4; however, the actual flight hardware is at TRL-6/7 allowing for an expedited component-level-testing [65]. The schedule in Figure 5 was developed utilizing NASA's systems engineering handbook and the U.S. Government approval process for contracts [66]. The MCR, which verifies the capabilities of LUNAR EMU, will be completed in Q1 of 2025, allowing for the system requirements and architecture, MDR, to be completed by Q1 of 2026. Two years of development are dedicated to the PDR of LUNAR EMU, followed by one and a half years for the CDR at Q2 of 2029. MBSE testing and Agile Methodologies will be integrated into the development and certification of LUNAR EMU to decrease downstream costs during production conforming to 2029 NASA production standards [67]. This allows for over two years of production and physical testing, with the earliest launch beginning in Q2 of 2032. This production timeline is extended to the 2033 deadline due to considerations of NASA budget cuts. At each

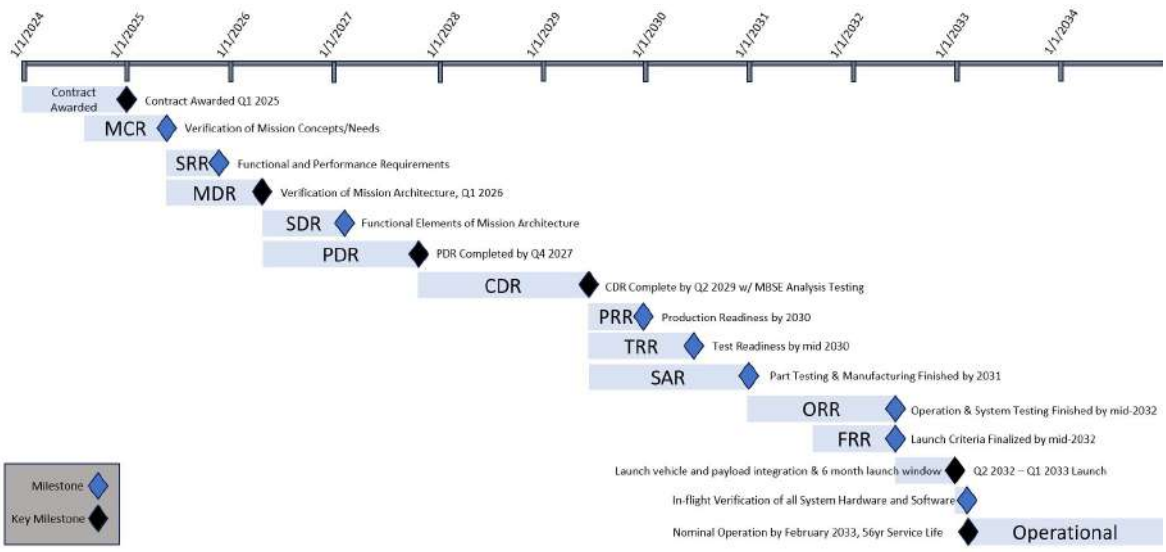


Figure 5: Production Schedule

step of the development process, LUNAR EMU will follow all manufacturing and testing standards outlined in Appendix M [68]. These range from circuit board analysis, grounding development, acoustic and shock testing, and fuel leak testing.

# 4 Conclusion

LUNAR EMU is a TRL-3 dual rover architecture, aimed to efficiently and effectively find ice, Helium-3 (He3), and other rare minerals and resources on the lunar south pole. Its overall objective is to assist the Artemis Missions by establishing a sustained human presence at the lunar south pole. LUNAR EMU's design utilises a combination of flight-tested technologies with the revolutionary integration of modern systems to optimise the rover for operation in the harsh environmental conditions it will experience.

Hydrogen fuel cell technology was selected over more common energy sources due to the recent failure of ISRO Chandrayaan-3 unable to make it through the dark cycle of the moon using solar panels and high density LiPo batteries [69]. It is possible the upcoming ISRO/JAXA Chandrayaan-4 and NASA VIPER will suffer the same fate due to the similar power sources [70, 16]. Radioisotope decay was omitted due to high costs. Therefore flight proven hydrogen fuel cells were selected, allowing for continuous operation inside the permanently shadowed craters without needing to emerge for recharging, providing a more efficient rover design than ISRO Chandrayaan-3, ISRO/JAXA Chandrayaan-4, and NASA VIPER [71, 72].

Over its 56 year lifespan it is capable of travelling a distance of 464.8km, whilst carrying all vital scientific equipment onboard for accurately determining the composition of all collected samples. The LUNAR EMU mission has a projected lifetime cost of $212.6 million USD, averaging out to $3.8 million USD per year over the duration of the mission. It's high TRL design has classified it as ready for launch before 2033, which would allow it to effectively fulfill its supporting role to the Artemis Missions as a large scale lunar crater prospector.

By embracing modern technological advancements in flight proven hardware and technology, LUNAR EMU can continue to push the boundaries of lunar exploration, paving the way for unprecedented scientific discoveries and advancements in space exploration.

# A Works Cited

# References


[1] ESA. "Helium-3 Mining on the Lunar Surface". In: *European Space Agency* (2023). URL: https://www.esa.int/Enabling_Support/Preparing_for_the_Future/Space_for_Earth/Energy/Helium-3_mining_on_the_lunar_surface.

[2] Florian Vidal and French Institute of International Relations. "Helium-3 from the Lunar Surface for Nuclear Fusion". In: *Polytechnique insights* (2022). URL: https://www.polytechnique-insights.com/en/braincamps/space/extraterrestrial-mining/helium-3-from-the-lunar-surface-for-nuclear-fusion/.

[3] Daniel Johnson. "Meet Shackleton Crater: Future Moon Landing Site". In: *Sky & Telescope* (2022). URL: https://skyandtelescope.org/astronomy-news/meet-shackleton-crater-moon-landing-site/.

[4] Dr. Paul D. Spudis. "Poles of the Moon". In: *Lunar and Planetary Institute* (2023). URL: https://www.lpi.usra.edu/science/moonPoles/.

[5] David Paige. "Science". In: *LRO DIVINER Lunar Radiometer Experiment* (2023). URL: https://www.diviner.ucla.edu/science.

[6] Jacob Knutson. "NASA Shares Unprecedented View of Moon's South Pole Region". In: *Axios* (2023). URL: https://www.axios.com/2023/09/19/nasa-moon-image-shackleton-crater-ice.

[7] E. Sefton-Nash et al. "Evidence for Ultra-cold Traps and Surface Water Ice in the Lunar South Polar Crater Amundsen". In: *Icarus* 332 (2019), pp. 1–13. ISSN: 0019-1035. DOI: https://doi.org/10.1016/j.icarus.2019.06.002. URL: https://www.sciencedirect.com/science/article/abs/pii/S0019103518306328.

[8] C.C. Allen and NASA Johnson Space Center. "Lunar Crater Observing and Sensing Satellite Site Selection – Showmaker Crater". In: *National Aeronautics and Space Administration* (2023). URL: https://www.lpi.usra.edu/meetings/lcross2006/pdf/9001.pdf.

[9] Anthony Colaprete et al. "Detection of Water in the LCROSS Ejecta Plume". In: *Science* 330.6003 (2010), pp. 463–468. DOI: 10.1126/science.1186986. URL: https://www.science.org/doi/abs/10.1126/science.1186986.

[10] SMD Content Editors. "LCROSS". In: *National Aeronautics and Space Administration* (2023). URL: https://science.nasa.gov/mission/lcross/.

[11] Joel Raupe. "Postdoctoral Position at UCLA (LRO Diviner)". In: *Lunar Networks* (2012). URL: https://lunarnetworks.blogspot.com/2012/02/postdoctoral-position-at-ucla-lro.html.

[12] MatWeb. "Aluminum 2219-T62". In: *ASM Aerospace Specification Metals Inc.* (2023). URL: https://asm.matweb.com/search/SpecificMaterial.asp?bassnum=ma2219t62.

[13] Dr. David R. Williams and NASA Goddard Space Flight Center. "The Apollo Lunar Roving Vehicle". In: *National Aeronautics and Space Administration* (2016). URL: https://nssdc.gsfc.nasa.gov/planetary/lunar/apollo_lrv.html.

[14] B.D. Dunn et al. "The corrosion properties of Spacelab structural alloy aluminium 2219 - T851". In: *European Space Agency* (May 1984). ISSN: 0379-4067. URL: http://esmat.esa.int/publications/published_papers/esa_str-212.pdf.

[15] Hadomei Aluminum CO. "The Application of 2219 Aluminum in Aerospace Industry". In: *Hadomei Aluminum* (2020). URL: https://www.aircraftaluminium.com/a/the-application-of-2219-aluminum-in-aerospace-industry.html.

[16] NASA. "Viper – Volatiles Investigating Polar Exploration Rover". In: *National Aeronautics and Space Administration* (2023). URL: https://science.nasa.gov/mission/viper/.

[17] Martin Volz. "Aluminum 2195 T8 Gore Development for Space Launch System Core and Upper Stage". In: *George C. Marshall Space Flight Center Research and Technology Report 2014* (Jan. 2015). URL: https://ntrs.nasa.gov/citations/20160008018.

[18] MatWeb. "2195 Aluminum Composition Spec". In: *MatWeb* (2023). URL: https://www.matweb.com/search/datasheet_print.aspx?matguid=4363dafc7f5545688506d8b4af1e9468.

[19] Bo-yong He, Sheng-gan Wu, and Heng-nian Li. "Reachable Set Analysis of Practical Trans-lunar Orbit via a Retrograde Semi-analytic Model". In: *Earth, Planets and Space* (2023). DOI: https://doi.org/10.1186/s40623-023-01782-y. URL: https://earth-planets-space.springeropen.com/counter/pdf/10.1186/s40623-023-01782-y.pdf.

[20] NASA. "Perseverance Rover". In: *National Aeronautics and Space Administration – Jet Propulsion Laboratory* (2023). URL: https://www.jpl.nasa.gov/news/press_kits/mars_2020/launch/mission/spacecraft/perseverance_rover/.

[21] NASA. "Curiosity's Sky Crane Maneuver, Artist's Concept". In: *National Aeronautics and Space Administration* (2011). URL: https://www.nasa.gov/image-article/curiositys-sky-crane-maneuver-artists-concept/.

[22] NASA. "Final Minutes of Curiosity's Arrival at Mars". In: *National Aeronautics and Space Administration* (July 2010). URL: https://www.nasa.gov/image-article/final-minutes-of-curiositys-arrival-mars/.

[23] Mars Communications Team at NASA's Jet Propulsion Laboratory. "Mars Curiosity Rover - Electrical Power". In: *NASA Science Mars Exploration* (2023). URL: https://mars.nasa.gov/msl/spacecraft/rover/power/.

[24] Mars Communications Team at NASA's Jet Propulsion Laboratory. "Power Source". In: *NASA Science Mars 2020 Mission Perseverance Rover* (2023). URL: https://mars.nasa.gov/mars2020/spacecraft/rover/electrical-power/.

[25] James Elmer Werner et al. "Cost Comparison in 2015 Dollars for Radioisotope Power Systems – Cassini and Mars Science Laboratory". In: *U.S. Department of Energy Office of Scientific and Technical Information* (July 2016). DOI: 10.2172/1364515. URL: https://www.osti.gov/biblio/1364515.

[26] Nautilus. "The Comparison of Different Technologies for On-board Power Supply of Cruise Ships". In: *Nautilus* (2023). URL: https://nautilus-project.eu/news/the-comparison-of-different-technologies-for-on-board-power-supply-of-cruise-ships.

[27] U.S. Department of Energy. "Types of Fuel Cells". In: *Office of Energy Efficiency & Renewable Energy* (2024). URL: https://www.energy.gov/eere/fuelcells/types-fuel-cells.

[28] Office of Energy Efficiency & Renewable Energy. "Hydrogen Storage". In: *Hydrogen and Fuel Cell Technologies Office* (2024). URL: https://www.energy.gov/eere/fuelcells/hydrogen-storage.

[29] Mars Communications Team at NASA's Jet Propulsion Laboratory. "Where is Perseverance?" In: *NASA Science Mars 2020 Mission Perseverance Rover* (2023). URL: https://mars.nasa.gov/mars2020/mission/where-is-the-rover/.

[30] Andrew Good, Karen Fox, and Alana Johnson. "10 Years Since Landing NASA's Curiosity Mars Rover Still Has Drive". In: *NASA Science MARS Exploration* (2023). URL: https://mars.nasa.gov/news/9240/10-years-since-landing-nasas-curiosity-mars-rover-still-has-drive/.

[31] Concha M. Reid et al. "Advanced Lithium-Ion Cell Development for NASA's Constellation Missions". In: *NASA Glenn Research Center* (2008). URL: https://ntrs.nasa.gov/api/citations/20130013133/downloads/20130013133.pdf.

[32] Diana Fitzgerald and John Gould. "NASA's Solid-State Battery Research Exceeds Initial Goals Draws Interest". In: *National Aeronautics and Space Administration* (2022). URL: https://www.nasa.gov/aeronautics/nasas-solid-state-battery-research-exceeds-initial-goals-draws-interest/.

[33] R. Kanno. "SECONDARY BATTERIES – LITHIUM RECHARGEABLE SYSTEMS — Electrolytes: Solid Sulfide". In: *Encyclopedia of Electrochemical Power Sources*. Ed. by Jürgen Garche. Amsterdam:

Elsevier, 2009, pp. 129–137. ISBN: 978-0-444-52745-5. DOI: https://doi.org/10.1016/B978-044452745-5.00212-4. URL: https://www.sciencedirect.com/science/article/pii/B9780444527455002124.

[34] S. Mathias. "Spaceborne Passive Radiative Cooler". In: *NASA Technical Reports Server* (1993). URL: https://ntrs.nasa.gov/citations/19930019613.

[35] Burt Zhang, Melora Larson, and Jose Rodriguez. "Passive coolers for pre-cooling of JT loops for deep space infrared imaging applications". In: *Cryogenics* 50.9 (2010). 2009 Space Cryogenic Workshop, pp. 628–632. ISSN: 0011-2275. DOI: https://doi.org/10.1016/j.cryogenics.2010.02.019. URL: https://www.sciencedirect.com/science/article/pii/S0011227510000585.

[36] Yukon Group. "Thermal Sensitivity NETD (Noise Equivalent Temperature Difference)". In: *PULSAR* (2024). URL: https://www.pulsar-nv.com/glo/support/thermal-imaging-technologies/thermal-sensitivity-netd-noise-equivalent-temperature-difference/2233/.

[37] Nancy Smith Kilkenny and NASA Glenn Research Center. "Reinventing the Wheel". In: *National Aeronautics and Space Administration* (Oct. 2017). URL: https://www3.nasa.gov/specials/wheels/.

[38] David Stowe et al. "Designing a Lunar Wheel". In: (Jan. 2008). DOI: 10.1115/DETC2008-49981.

[39] Sarah Morgan. "Reinventing the wheel for lunar rover". In: *Insitiute of Materials, Minerals & Mining* (Sept. 2023). URL: https://www.iom3.org/resource/reinventing-the-wheel-for-lunar-rover.html.

[40] Kiyohide Yasuhara. "Improvement of the wheel design of lunar mobility". In: *Operating in the Lunar Environment* (Feb. 2021). URL: https://tothemoon.pubpub.org/pub/g55irn1h.

[41] Vivake Asnani, Damon Delap, and Colin Creager. "The Development of Wheels for the Lunar Roving Vehicle". In: *National Aeronautics and Space Administration, Glenn Research Center, Cleveland, Ohio* (Dec. 2009). URL: https://ntrs.nasa.gov/api/citations/20100000019/downloads/20100000019.pdf.

[42] Pablo Abad-Manterola et al. "Axel Rover Paddle Wheel Design, Efficiency, and Sinkage on Deformable Terrain". In: *2010 IEEE International Conference on Robotics and Automation* (May 2010). URL: http://vigir.missouri.edu/~gdesouza/Research/Conference_CDs/IEEE_ICRA_2010/data/papers/1992.pdf.

[43] Wanshen Xiao and Yan Zhang. "Design of manned lunar rover wheels and improvement in soil mechanics formulas for elastic wheels in consideration of deformation". In: *Journal of Terramechanics* 65 (2016), pp. 61–71. ISSN: 0022-4898. DOI: https://doi.org/10.1016/j.jterra.2016.03.004. URL: https://www.sciencedirect.com/science/article/pii/S0022489816300027.

[44] Abby Tabor and NASA's Ames Research Center. "Artemis Moon Rover's Wheels are Ready to Roll". In: *National Aeronautics and Space Administration* (July 2023). URL: https://www.nasa.gov/solar-system/artemis-moon-rovers-wheels-are-ready-to-roll/.

[45] NASA. "The [Viper] Rover and its Onboard Toolkit". In: *National Aeronautics and Space Administration* (2023). URL: https://science.nasa.gov/mission/viper/rover-and-instruments/.

[46] Dr. David R. Williams and NASA Goddard Space Flight Center. "Ice on the Moon – A summary of Clementine and Lunar Prospector Results". In: *National Aeronautics and Space Administration* (2022). URL: https://nssdc.gsfc.nasa.gov/planetary/ice/ice_moon.html.

[47] Charles Malespin and NASA's Goddard Space Flight Center. "Mars Curiosity Rover – SAM". In: *National Aeronautics and Space Administration – Jet Propulsion Laboratory* (2023). URL: https://mars.nasa.gov/msl/spacecraft/instruments/sam/.

[48] ESA. "Optical Properties of Ice and Snow". In: *European Space Agency* (2013). URL: https://www.esa.int/SPECIALS/Eduspace_Global_EN/SEMPJ7TWLUG_2.html.

[49] NASA. "Lunar Reconnaissance Orbiter". In: *National Aeronautics and Space Administration* (2023). URL: https://science.nasa.gov/mission/lro/.

[50] Magdalena. "Fleet Space Technologies to Revolutionize Mineral Exploration with Launch of ExoSphere". In: *Fleet* (2022). URL: https://fleetspace.com/news/fleet-space-technologies-to-revolutionise-mineral-exploration-with-launch-of-new-solution.

[51] European Space Agency. "Satellite frequency bands". In: *European Space Agency* (2024). URL: https://www.esa.int/Applications/Connectivity_and_Secure_Communications/Satellite_frequency_bands.

[52] NASA. "Electromagnetics". In: *National Aeronautics and Space Administration* (2023). URL: https://science.nasa.gov/learn/basics-of-space-flight/chapter6-3/.

[53] Philipp Zanon, Michelle Dunn, and Geoffrey Brooks. "Current Lunar dust mitigation techniques and future directions". In: *Acta Astronautica* 213 (2023), pp. 627–644. ISSN: 0094-5765. DOI: https://doi.org/10.1016/j.actaastro.2023.09.031. URL: https://www.sciencedirect.com/science/article/pii/S0094576523004939.

[54] Yinhu Zhan, Shaojie Chen, and Xu Zhang. "Adaptive celestial positioning for the stationary Mars rover based on a self-calibration model for the star sensor". In: *Journal of Navigation* 75.1 (2022), pp. 160–175. DOI: 10.1017/S0373463321000680. URL: https://www.cambridge.org/core/journals/journal-of-navigation/article/abs/adaptive-celestial-positioning-for-the-stationary-mars-rover-based-on-a-selfcalibration-model-for-the-star-sensor/A2D6BAC2411F883FE6D85202E847CEFB.

[55] Jonathan D. Gammell et al. "Rover Odometry Aided by a Star Tracker". In: *Institute for Aerospace Studies - University of Toronto* (2013). URL: http://asrl.utias.utoronto.ca/~jdg/sbib/gammell_ieeeac13.pdf.

[56] V. Verma et al. "Autonomous robotics is driving Perseverance rover's progress on Mars". In: *National Library of Medicine* (2023). DOI: 10.1126/scirobotics.adi3099. URL: https://pubmed.ncbi.nlm.nih.gov/37494463/.

[57] Tina Hilding, Voiland College of Engineering, and Architecture. "Liquid Nitrogen Spray Could Clean up Stubborn Moon Dust". In: *Washington State University Insider* (2023). URL: https://news.wsu.edu/press-release/2023/02/28/liquid-nitrogen-spray-could-clean-up-stubborn-moon-dust/.

[58] M. A. Kreslavsky and III Head J. W. "The Steepest Slopes on the Moon: Gradual Degradation and Instant Removal by Basin-Forming Impacts". In: 2015, P53B-2126 (Dec. 2015), P53B–2126. URL: https://ui.adsabs.harvard.edu/abs/2015AGUFM.P53B2126K/abstract.

[59] Jane Platt and NASA Science Mars 2020 Mission Perseverance Rover. "Mission FAQs". In: *NASA Science Mars 2020 Mission Perseverance Rover* (2023). URL: https://mars.nasa.gov/mars2020/mission/faq/.

[60] Eric Berger. "Inside Elon Musk's plan to build one Starship a week—and settle Mars". In: *ArsTECHNICA* (2020). URL: https://arstechnica.com/science/2020/03/inside-elon-musks-plan-to-build-one-starship-a-week-and-settle-mars/.

[61] The Planetary Society. "Cost of MSL Curiosity". In: *The Planetary Society* (2023). URL: https://www.planetary.org/space-policy/cost-of-msl-curiosity.

[62] The Planetary Society. "VIPER, NASA's Moon resource mapper". In: *The Planetary Society* (2024). URL: https://www.planetary.org/space-missions/viper.

[63] Jeff Foust. "NASA delays VIPER lunar rover launch by a year". In: *SpaceNews* (2022). URL: https://spacenews.com/nasa-delays-viper-lunar-rover-launch-by-a-year/.

[64] SpaceX. "Falcon Heavy". In: *SpaceX* (2024). URL: https://www.spacex.com/vehicles/falcon-heavy/.

[65] Catherine G. Manning. "Technology Readiness Levels". In: *National Aeronautics and Space Administration* (Sept. 2023). URL: https://www.nasa.gov/directorates/somd/space-communications-navigation-program/technology-readiness-levels/.

[66] NASA. "NASA Systems Engineering Handbook". In: *National Aeronautics and Space Administration* (2007). URL: https://www.nasa.gov/wp-content/uploads/2018/09/nasa_systems_engineering_handbook_0.pdf.

[67] Karen J. Weiland and Glenn Research Center. "Future Model-Based Systems Engineering Vision and Strategy Bridge for NASA". In: *National Aeronautics and Space Administration* (Oct. 2021). URL: https://ntrs.nasa.gov/api/citations/20210014025/downloads/TM-20210014025.pdf.

[68] Brenda Bailey. "Standards from All Technical Disciplines". In: *National Aeronautics and Space Administration* (2023). URL: https://standards.nasa.gov/all-standards.

[69] Department of Space Indian Space Research Organization. "LVM3-M4-Chandrayaan-3 Mission". In: *Indian Space Research Organization, Department of Space* (2023). URL: https://www.isro.gov.in/Chandrayaan3.html.

[70] HT TECH. "Chandrayaan-4 Mission: ISRO-JAXA Plans for Lunar Mission". In: *HT TECH* (2023). URL: https://tech.hindustantimes.com/photos/chandrayaan4-mission-isro-jaxa-plans-for-lunar-mission-71698819585884.html.

[71] Kenneth A. Burke and Glenn Research Center. "Fuel Cells for Space Science Applications". In: *National Aeronautics and Space Administration* (2003). URL: https://ntrs.nasa.gov/api/citations/20040010319/downloads/20040010319.pdf.

[72] National Air and Space Museum. "Fuel Cell, Apollo". In: *National Air and Space Museum* (2023). URL: https://airandspace.si.edu/collection-objects/fuel-cell-apollo/nasm_A19730934000.

[73] Dr. John Olsen. "Hydrogen Fuel Cell Lecture". In: *UNSW AERO9660 Mechanical and Manufacturing Engineering* (Oct. 2023).

[74] Clifford Atiyeh. "2024 Toyota Mirai". In: *Car and Driver* (2024). URL: https://www.caranddriver.com/toyota/mirai.

[75] Office of Energy Efficiency & Renewable Energy - Hydrogen and Fuel Cell Technology Office. "Hydrogen Shot". In: *U.S. Department of Energy* (2024). URL: https://www.energy.gov/eere/fuelcells/hydrogen-shot.

[76] "Pricing and Lead Time". In: *Pennsylvania State University* (2024). URL: https://generalstores.psu.edu/pricing-and-lead-time.

[77] "1/2 in. x 10ft. Copper Type L Pipe". In: *The Home Depot* (2024). URL: https://www.homedepot.com/p/Mueller-Streamline-1-2-in-x-10-ft-Copper-Type-L-Pipe-LH04010/100354232.

[78] "Nikon D5600 DSLR Camera with 18-140mm Lens". In: *Walmart* (2024). URL: https://www.walmart.com/ip/Nikon-D5600-DSLR-Camera-with-18-140mm-Lens/.

[79] Allied Vision. "Allied Vision Manta G-145 2/3" NIR CCD Camera". In: *EO Edmund Optics Worldwide* (2024). URL: https://www.edmundoptics.com/p/Allied-Vision-Manta-G-145-23-NIR-CCD-Camera/29709.

[80] IDS. "GV-5270SE-M-GL". In: *Wilco Imaging* (2024). URL: https://wilcoimaging.com/products/gv-5270se-m-gl?currency=USD.

[81] OPSIN. "Helmet-Mounted Monocular". In: *Sionyx* (2024). URL: https://www.sionyx.com/products/opsin?variant=40374006775878.

[82] Jean Folger, Somer Anderson, and Pete Rathburn. "Why Curiosity Cost $2.5 Billion". In: *Investopedia* (2022). URL: https://www.investopedia.com/financial-edge/0912/why-curiosity-cost-2.5-billion.aspx.

[83] "BLUEROCK GCD4 Gasoline Portable Handheld Core Drill - Honda 4-Stroke Gas Coring". In: *BlueRock* (2024). URL: https://www.bluerocktools.com/bluerock-gcd4-gasoline-portable-handheld-core-drill-honda-4-stroke-gas-coring/.

[84] Sick. "Sick 1066423 DL100-21HA2110 Long Range Distance Sensor". In: *Southern Electronics* (2024). URL: https://southernele.com/sick-1066423-dl100-21ha2110-long-range-distance-sensor/.

[85] LiperiAir. “LiperiAir Semi Solid State 22000mAh 12S 10C 44.4V Lipo Battery Pack With XT90 Plug”. In: *RCBattery* (2024). URL: https://rcbattery.com/liperiair-semi-solid-state-22000mah-12s-10c-44-4v-lipo-battery-pack-with-xt90-plug.html.

[86] “Broadband Gain Horn Antenna Operating from 1 GHz to 18 GHz with a Nominal 0 dBi Gain and SMA Female Input”. In: *Fairview Microwave* (2024). URL: https://www.fairviewmicrowave.com/invalid-alias-waveguide-horn-antenna-none-flange-11dbi-18-ghz-sh0118s-p.aspx.

[87] “MOTIV 434B Matic Rim 18X7.5 5x108/5x112 Offset 40 Gloss Black (Quantity of 1)”. In: *ebay* (2024). URL: https://www.ebay.com/itm/184962322639.

[88] “Torsion Bar”. In: *Rod End Supply* (2024). URL: https://rodendsupply.com/shop/torsion-bar/.

[89] University of Arkansas. “Liquid Nitrogen Price List”. In: *Business Services Procurement* (2024). URL: https://procurement.uark.edu/e-procurement/liquid-nitrogen-price-list.php.

[90] “Aluminum Sheet 2219-T851 1.5” (t)”. In: *Buymetal.com* (2024). URL: https://store.buymetal.com/aluminum-sheet-2219-t851-1-5.html.

[91] SpaceX. “Capabilities & Services”. In: *Way Back Machine* (2024). URL: https://web.archive.org/web/20220322170331/https://www.spacex.com/media/Capabilities%5C&Services.pdf.

# B Acronym List

| Acronym | Meaning |
|---|---|
| AI | Artificial Intelligence |
| AIAA | American Institute of Aeronautics and Astronautics |
| AL2195 | Aluminum Alloy 2195 |
| Al2219 | Aluminum Alloy 2219 |
| Alt | Altitude |
| AOI | Area of Interest |
| Az | Azimuth |
| CAD | Computer Aided Design / Drafting |
| Caltech | California Insutute of Technology |
| CDR | Critical Design Review |
| COMM | Communication |
| DC | Direct Current |
| DEB | Dynamic Eclipse Broadcast |
| DSN | Deep Space Network |
| ELO2 | EPE + Lunar Outpost Oceania Consortium |
| EMU | Energetic Mining Unit |
| ESA | European Space Agency |
| FEA | Finite Element Analysis |
| FOS | Factor of Safety |
| FRR | Flight Readiness Review |
| GPS | Global Positioning System |
| H2 | Hydrogen |
| He3 | Helium-3 |
| HEO | Highly Elliptical Orbit |
| ISRO | Indian Space Research Organisation |
| JAXA | Japan Aerospace Exploration Agency |
| JPL | Jet Propulsion Laboratory |
| LCROSS | Lunar Crater Observation and Sensing Satellite |
| LEMU | Little EMU |
| LEO | Low Earth Orbit |
| LH2 | Liquid Hydrogen |
| LiPo | Lithium-Polymer |
| LN2 | Liquid Nitrogen |
| LO2 / LOX | Liquid Oxygen |
| LRO | Lunar Reconnaissance Orbiter |
| LRV | Lunar Roving Vehicle |
| LUNAR EMU | Long-range Unmanned New Artemis Rover Electric Mining Unit |
| MBSE | Model Based Systems Engineering |
| MCR | Mission Concept Review |
| MDR | Mission Definition Review |
| ML | Machine Learning |
| NASA | National Aeronautics and Space Administration |
| NAV | Navigation |
| NETD | Noise Equivalent Temperature Difference |

| | |
|---|---|
| NIR | Near Infrared Radiation |
| O2 | Oxygen |
| ODE | Ordinary Differential Equation |
| OPIR | Overhead Persistent Infrared Radiation |
| ORR | Operational Readiness Review |
| PDR | Preliminary Design Review |
| PEM | Proton Exchange Membrane / Polymer Electrolyte Membrane |
| PRC | Passive Radiative Cooler |
| PROF | Professor |
| PRR | Production Readiness Review |
| PSR | Permanently Shadowed Region |
| RASC-AL | Revolutionary Aerospace Systems Concepts – Academic Linkage |
| rpm | Rotations per Minute |
| RTG | Radioisotope Thermoelectric Generator |
| SABERS | Solid-state Architecture Batteries for Enhanced Rechargeability and Safety |
| SAM | Sample Analysis at Mars tool |
| SAR | System Acceptance Review |
| SDR | System Design Review |
| SLS | Space Launch System |
| SRR | System Requirements Review |
| STEM | Science, Technology, Engineering, and Mathematics |
| SWIR | Short Wave Infrared Radiation |
| TA | Teaching Assistant |
| TRL | Technical Readiness Level |
| TRR | Test Readiness Review |
| UCCS | University of Colorado, Colorado Springs |
| UE5 | Unreal Engine 5 |
| UGRD | Undergraduate |
| UNSW | University of New South Whales |
| US / U.S. | United States of America |
| USD | United States Dollar |
| V&V | Verification and Validation |
| VIPER | Volatiles Investigating Polar Exploration Rover |
| WMC | World Mining Congress |

# C PEM Fuel Cell Diagram

Depicted below is the schematic for an individual PEM fuel cell. Hydrogen ($H_2$) and Oxygen ($O_2$) are fed into a membrane, splitting the oxygen atoms while removing the hydrogen electron. In turn, this creates electricity from the electrons moving from the anode to cathode, while creating water ($H_2$) as a byproduct.

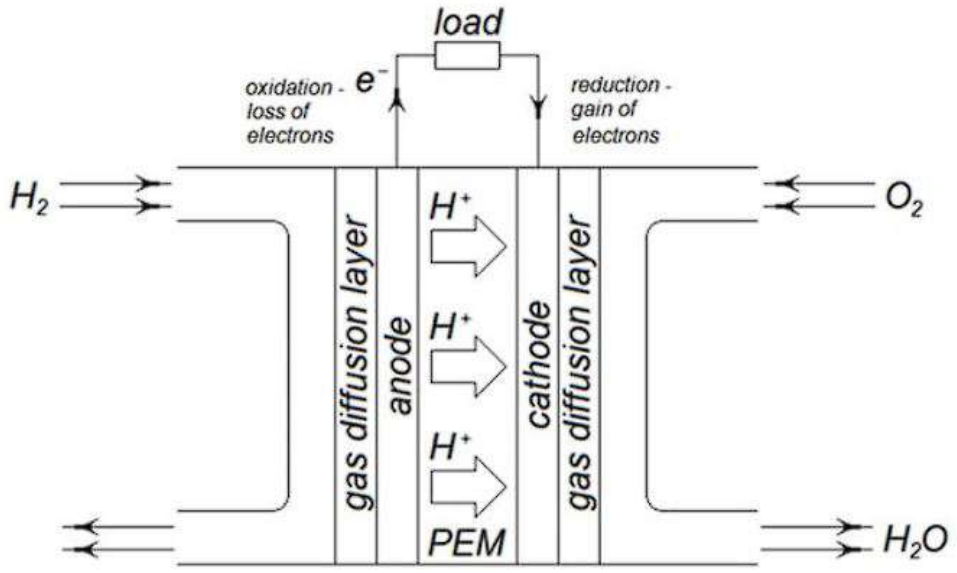


Figure 6: Schematic of an Individual PEM Cell [73]

# D Hydrogen Fuel Cell Stack Statistics

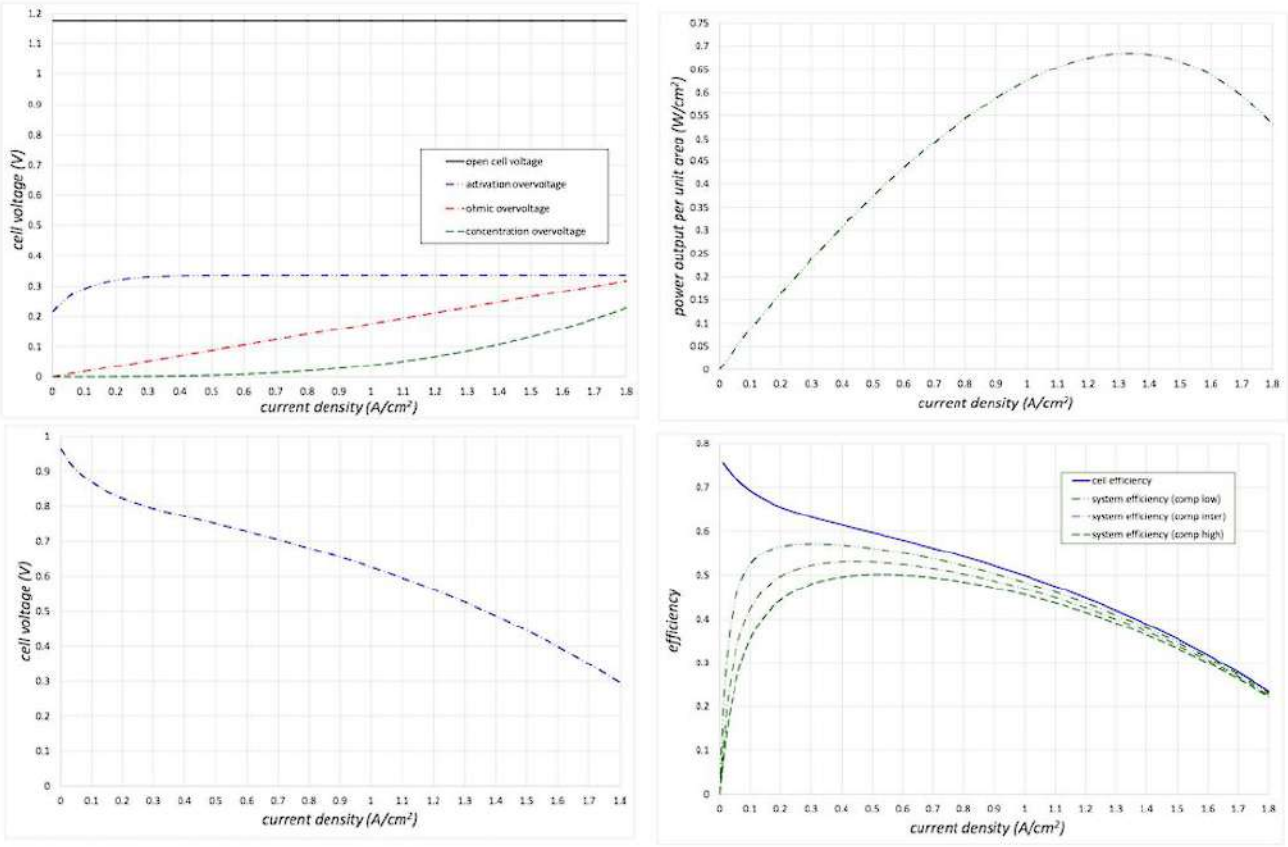


Figure 7: PEM Fuel Cell Stack Statistics

Figure is derived from an UNSW AERO9660 lecture, given by Dr. John Olsen a faculty member of Mechanical and Manufacturing Engineering, given on October 25, 2023 [73]. The statistics are give per a single fuel cell unit, by stacking the fuel cells in parallel or series, more voltage or current, respectively, can be produced to produce large amounts of power in a relatively confined space.

# E Python CoolProp Code

Below shows the Python code utilized to determine the annual volumetric fuel consumption with fuel tank conditions for temperature $\in$ [55, 70]K and pressure $\in$ [1, 100]bar. The boundary conditions were based off of preliminary research on the average south pole surface temperature, and typical hydrogen fuel containment pressures.

```
### Basic H2 Fuel Tank Size ###
from CoolProp.CoolProp import PropsSI
import pandas as pd
from mpl_toolkits import mplot3d
import numpy as np
import matplotlib.pyplot as plt

## Initialize:
FOS = 3;
Distance_Req = FOS*11.8 # km/yr
Size_Array_H2 = []
Size_Array_O2 = []
Size_Array_Both = []
Temp_A = []
Press_A = []

## Knowns
eff = 131.57 #km/kg

## Fuel Tank Size
mass_H2 = Distance_Req/eff # kg/yr
mole_H2 = mass_H2/(2.061/1000) # mol
mole_O2 = mole_H2/2 # mol
mass_O2 = (31.999/1000)*mole_O2 # kg


for Temp in range(55, 70, 1): # Indexs thru Temp
    for Press in range(1*10**5, 100*10**5, 15*10**4): # Indexs thru Pressure
        Density_H2 = PropsSI('D', 'T', Temp, 'P', Press, 'Hydrogen') # kg/m^3
        Density_O2 = PropsSI('D', 'T', Temp, 'P', Press, 'Oxygen') # kg/m^3
        Density_H2 = Density_H2/1000 # kg/L
        Density_O2 = Density_O2/1000 # kg/L
        Size_H2 = mass_H2/Density_H2 # L/yr
        Size_O2 = mass_O2/Density_O2 # L/yr
        Size_Both = Size_H2 + Size_O2# L/yr
        Size_Array_H2.append(Size_H2)
        Size_Array_O2.append(Size_O2)
        Size_Array_Both.append(Size_Both)
        Temp_A.append(Temp)
        Press_A.append(Press)

df = pd.DataFrame({'Temperature [K]':Temp_A,'Pressure [10 bar]':Press_A, 'Size H2 [L]
    ↪ ':Size_Array_H2, 'Size O2 [L]':Size_Array_O2, 'Size Both [L]':Size_Array_Both})
df.to_excel("H2_Fuel_Tank_Size.xlsx")

## Hydrogen Figure
figH2 = plt.figure(figsize=(10,7))
ax = plt.axes(projection='3d')
ax.plot_trisurf(Temp_A, Press_A, Size_Array_H2, cmap='viridis')
ax.set_xlabel('Temperature [K]')
ax.set_ylabel('Pressure [10 bar]')
ax.set_zlabel('Size [L]')
ax.set_title('Size of H2 Fuel Tank')
```

```
plt.margins(0, tight=False)
ax.view_init(25,45)


## Oxygen Figure
figO2 = plt.figure(figsize=(10,7))
ax = plt.axes(projection='3d')
ax.plot_trisurf(Temp_A, Press_A, Size_Array_O2, cmap='viridis')
ax.set_xlabel('Temperature [K]')
ax.set_ylabel('Pressure [10 bar]')
ax.set_zlabel('Size [L]')
ax.set_title('Size of O2 Fuel Tank')
plt.margins(0, tight=False)
ax.view_init(25,45)

## Both Figure
figBoth = plt.figure(figsize=(10,7))
ax = plt.axes(projection='3d')
ax.plot_trisurf(Temp_A, Press_A, Size_Array_Both, cmap='plasma')
ax.set_xlabel('Temperature [K]')
ax.set_ylabel('Pressure [10 bar]')
ax.set_zlabel('Size [L]')
ax.set_title('Size of Total Fuel Tank')
plt.margins(0, tight=False)
ax.view_init(25,45)
```

Utilizing the Python code shown above, Figure 8 shows the combined H2/O2 fuel tank consumption. Below shows the individual fuel consumption for both LH2 and LO2 respectively.

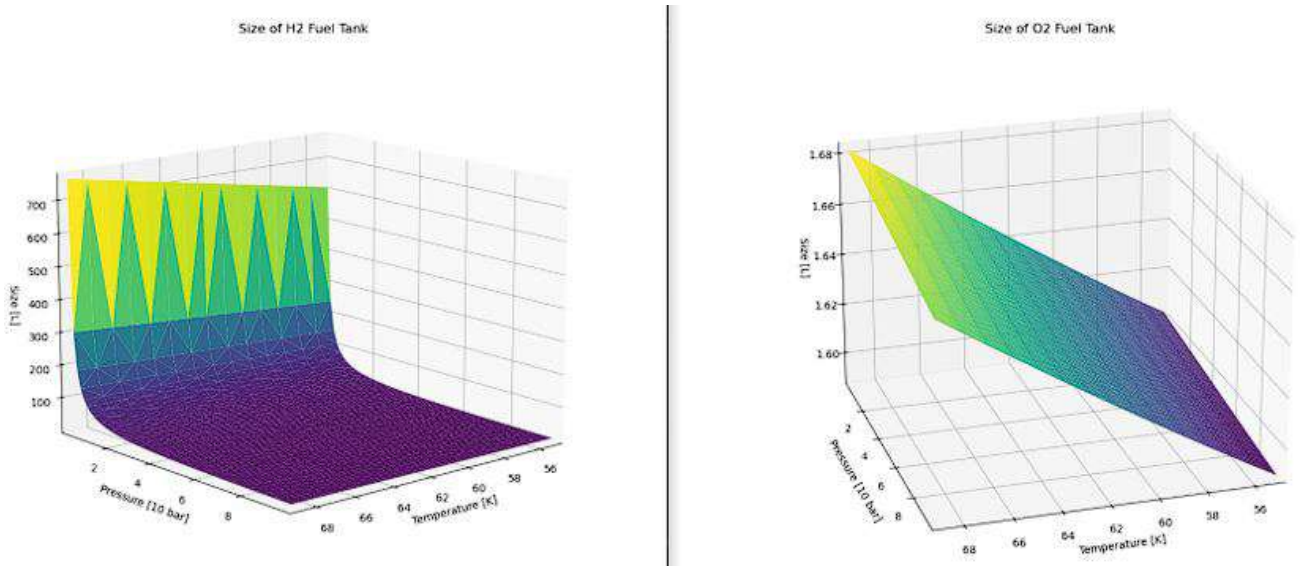


It can be noted that the LH2 fuel consumption exhibits an exponential growth as the pressure drops as it transitions from a liquid to gaseous state. LO2 meanwhile grows linearly, still in a liquid state, due the kinetic movement of the molecules decreasing the density as pressure drops and temperature rises.

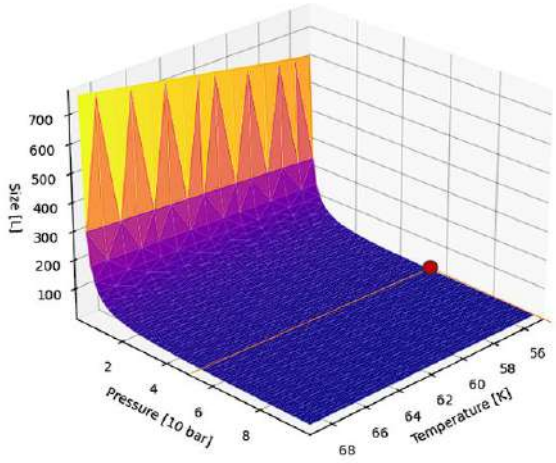


Figure 8: Annual Volumetric Fuel Consumption

The conditions for the fuel tank were optimized utilizing the Python code shown in Appendix E using the 'CoolProp' plugin, also featuring the annular fuel consumption for LO2 and LH2 individually. Figure 8 shows the total fuel tank size for only a single year of travel, where the red line and dot represents the initial fuel tank conditions. As fuel is drawn from the cryogenic state of the fuel tanks, the pressure drop across in fuel line will result in both fuels undergoing a phase change from a liquid to a gaseous state. Using an electronically controlled valve on each of the H2 and O2 fuel lines, the quantity of fuel entering the PEM can be controlled. Together, these maximize efficiency for the PEM fuel cell, as they work best utilizing gaseous fuels.

# F Propulsion Power Requirements

## F.1 Axel Power Requirements

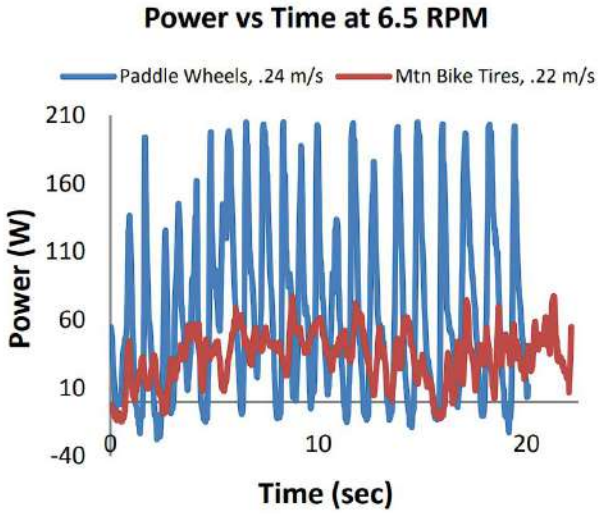


Figure of JPL and Caltech power requirement analysis to move their Axle paddle wheel at .24 $\frac{m}{s}$ along with a comperably sized mountain bike tire at .22 $\frac{m}{s}$ [42]. It can be noticed both trends are oscillatory in nature, however the Axel paddle wheel had triple the power requirement to a conventional tire and had an amplitude half of it's max power of 210W.

## F.2 Axel Power and Speed Relationship

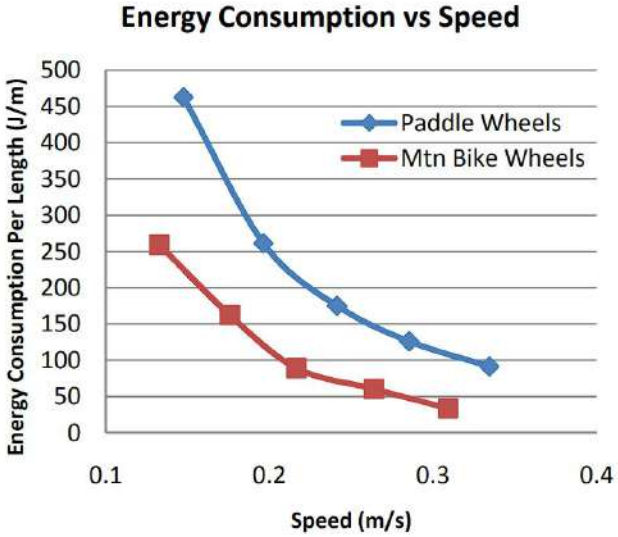


Figure of JPL and Caltech power and speed analysis to move their Axle paddle wheel and a comparable sized mountain bike tire [42]. Both data sets exponentially decrease as speed increase. Due ot the paddle wheel being very non-uniform, it has a much higher initial power requirement, but as speed increases, it decays faster than a more uniform tire into much lower power requirements.

## F.3 Generic Lugged Wheel Power Requirements

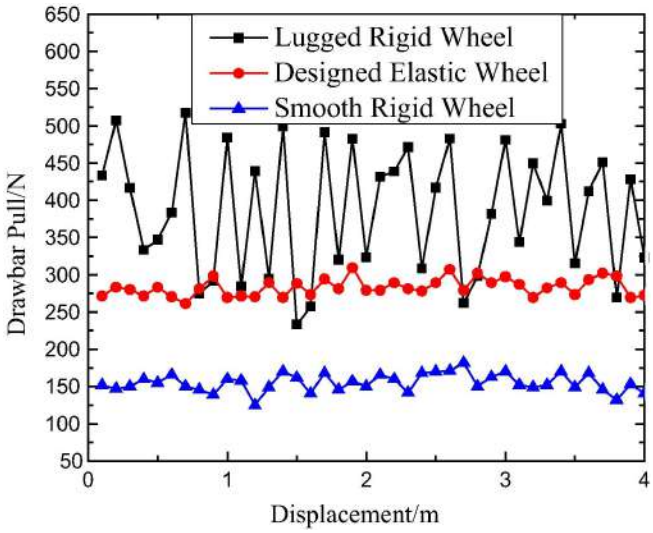


Figure of power requirements between a lugged, elastic, and rigid wheel [43]. Once more, it can be noted the lugged wheel has a very oscillatory power requirement due to it's geometrical non-uniformness. The elastic wheel had the second highest power requirements as the elastic wheel absorbed some of the kinetic energy in the form of potential energy.

## F.4 Generic Lugged Wheel Sinkage

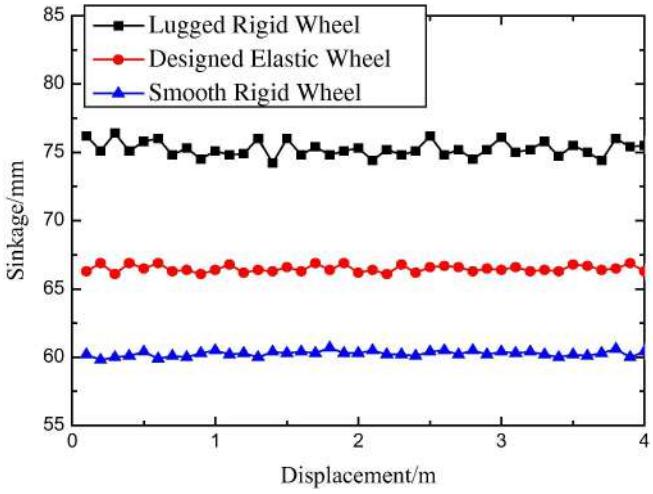


Figure of depth sinkage between a lugged, elastic, and rigid wheel [43]. The lugged wheel sunk the most into the soil, allowing it to achieve maximum traction at the expense of extra power, followed by the elastic wheel and finally the rigid wheel.

## F.5 Regolith Displacement

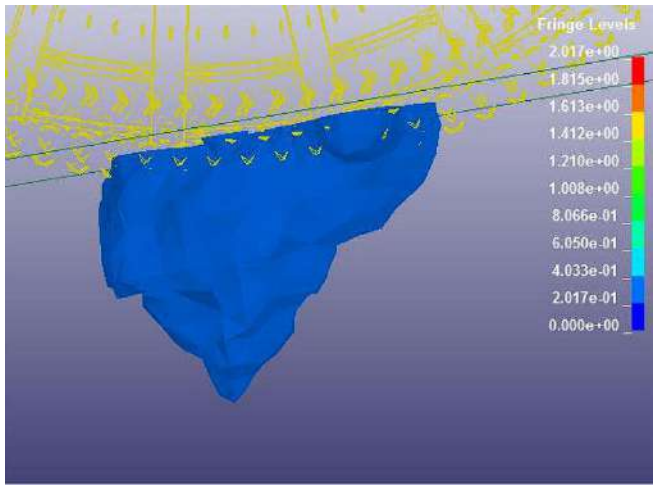


Graphical representation of the regolith sheer forces and displacement under the contact point of a rigid wheel from FEA [43]. The disturbed soil takes on a roughly conical shape under the point of contact. Using a lugged or an elastic wheel would increase the displacement of the soil, with a less focalized cone, decreasing the contact pressure and overall yielding more traction for the rover.

# G Electromagnetic Reflective Curve of Ice

Depicted below is the reflective curve of ice in the electromagnetic spectrum.

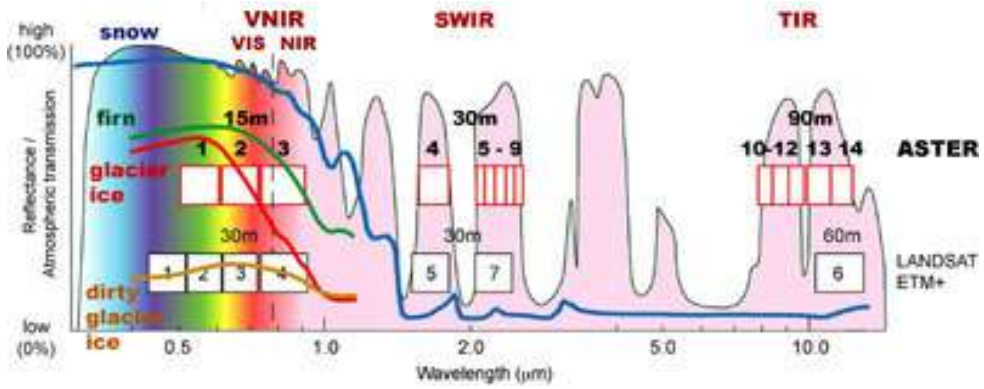


Figure 9: Electromagnetic Reflective Curve of Ice

# H EMU - LEMU Door Gearing Ratio

The following section of math was used to find the correct gearing ratio to not tip EMU from the torque and to ensure there was enough torque to lift the door using the 0.7 Nm 12rpm DC motor specifications.

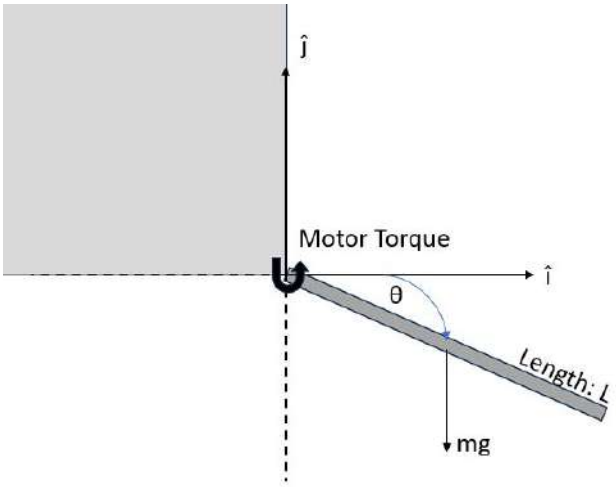


*2nd Area Mass Moment of Inertia* :
$I_0 = \frac{1}{12}ml^2 + m(\frac{l}{2})^2$

*Torque* :
$\tau = I\alpha$

*Substituting sum of Motor and Center of Mass Torque* : $\lambda$ *is used as a factor of gearing ratio*
$\tau = \lambda\frac{mgL}{2}cos\theta - \frac{mgL}{2}cos\theta = I\alpha$

*Solving as an ODE* : $\tau \geq 0$
$\tau = [\frac{1}{12}ml^2 + m(\frac{l}{2})^2]\ddot{\theta} + (1-\lambda)\frac{mgL}{2}cos\theta(t)$

This yielded a homogeneous, nonlinear, higher order differential equation, which is to complex to solve analytically. By assuming the motor will act as a step response, with the gear ratio reducing the angular acceleration, $\alpha$ was assumed to be near 0. The next simplification was the maximum motor torque will be imparted when the weight moment is maximized ($\theta = 0rad$). Using these two assumptions, and plugging in the material and physical properties, the following torques were created

$M_{max,Earth} = 41.9378\ Nm$
$M_{max,Moon} = 6.9253\ Nm$

For Earth this means that a 66:1 gear ratio would be required to lift the door using a single motor, or a 33:1 gear ratio using two motors, of 12V and 0.7Nm specifications. However, this drops to a 9:1 gear ratio for a single motor on the moon. The 33:1 gear ratio was kept as a large over-estimate to account for the non-zero moment of inertia and dust accumulation. Due to the high gearing ratios, it proves that the assumption of near-zero moment of inertia and angular acceleration was correct to make, as it essentially proved itself.

# I Unreal Engine 5 Photo-realistic Renders

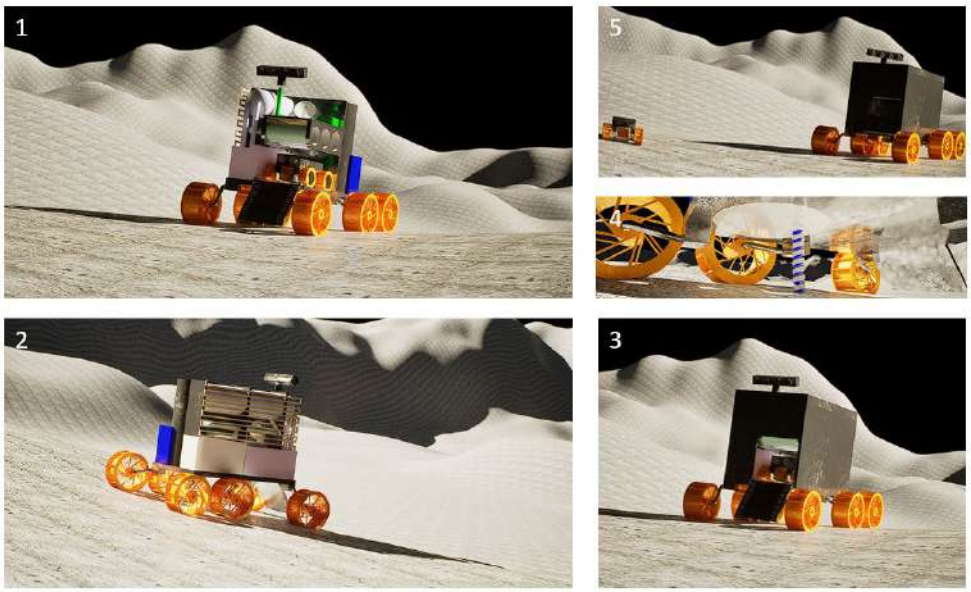


Figure 10: Unreal Engine 5 Renders

Figure 10 depicts five photo-realistic renders of the LUNAR EMU architecture utilizing Unreal Engine 5 (UE5). Images 1 and 2 are in the style of a cutaway illustration, with the rovers shell removed to depict the internal subsystems described in Figure 4. Image 3 depicts the LEMU stowage bay door opening, allowing LEMU to depart EMU and perform its independent mission requirements. Image 4 illustrates the drill and turntable (white) from underneath the rover. Image 5 shows both LEMU and EMU in their full active mission configuration.

# J Verification and Validation

Model Based Systems Engineering Verification and Validation (MBSE V&V) was used in order to analytically and systematically determine the operational state of the conceptual rover. Appendix J.1, dictating the requirements, was used to guide the creation of what is now LUNAR EMU. Meanwhile J.2 below, shows the analytical test to fulfill each requirement.

## J.1 Requirements List

| # | Requirement |
|---|---|
| 001 | Operate within a crater for at least a year |
| 002 | Travel 11.8km using data from previous missions |
| 003 | Operate for a year in complete darkness |
| 004 | Operate in temps of 60 - 400K |
| 005 | Operational by 2033 |
| 006 | Reliable source of energy for duration of operation |
| 007 | Withstand extreme temperature swings |
| 008 | Operate in micro-gravity, i.e. does not require gravity |
| 009 | Weighs less than 500lbs |
| 010 | Budget of $3 million |
| 011 | Protection from static regolith for electronic devices |
| 012 | Ability to house scientific equipment |
| 013 | Ability to locate and confirm ice/water |
| 014 | Ability to locate other substances within the crater |
| 015 | Ability to Geo-locate |
| 016 | Autonomous Navigation |
| 017 | Communication to the Deep Space Network and Satellites |
| 018 | Ability to get traction in the loose regolith in slopes of 45 degrees |
| 019 | Travel 1.5x the average rock size |
| 020 | Size requirement of 2m x 2m x 2m |

Requirements list generated to aid our process in designing the rover. LUNAR EMU meets all requirements except for Requirements 009 and 010 due to a lack of experience on developing space technologies. However, best efforts were made to satisfies the requirements as much as possible. Preliminary research on previous, current, and upcoming lunar rovers developed the requirements list on what it means for our rover to be feasible on the lunar surface.

## J.2 Requirement Analysis Tests

Below shows the requirement tests and passing criteria in order to show the requirements were fulfilled. Analysis tests were determined using mathematics, inspection tests were determined on if LUNAR EMU had the requirement integrated into the design, and Research tests are conceptual designs that would work but cannot by determined utilizing CAD software and requires in-field testing to pass by inspection.

| # | Test(s) | Passing Criteria | Result |
|---|---|---|---|
| 001 | Analysis | Travel 7.8km/yr utilizing the efficiency of $131.57\frac{km}{kg}$ of H2 | Pass by Section 2.1 |
| 002 | Analysis | Travel 11.8km utilizing the efficiency of $131.57\frac{km}{kg}$ of H2 | Pass by Section 2.1 |
| 003 | Inspection | Non-dependent of Sun line of sight | Pass Section 2.1 |
| 004 | Research | Material and power-systems can operate in 40-600K | Pass by Sections 2 |
| 005 | Inspection | TRL of all systems are greater than TR-L6 | Pass by Section 1 |
| 006 | Inspection | Independent Power Source | Pass by Section 2.1 |
| 007 | Research | Material and power-systems can operate in 40-600K | Pass by Sections 2 |
| 008 | Inspection | Non-gravity dependent | Pass by Section 2 |
| 009 | Analysis | Weighs less than 500 lbs | Fail by Section 2.9.3 |
| 010 | Analysis | Costs less than $3 Million USD | Fail by Section 3 |
| 011 | Inspection<br>Research | Vulnerable areas are protected from dust<br>Material deters dust | Pass by Sections 2, 2.7 |
| 012 | Inspection | LUNAR EMU Contains multiple scientific instruments | Pass by Sections 2.4.1, 2.4.2 |
| 013 | Inspection & Research | Contains necessary equipment to find water ice | Pass by Sections 2.4.1, 2.4.2 |
| 014 | Inspection & Research | Contains necessary equipment to find non-ice substances | Pass by Sections 2.4.1, 2.4.2 |
| 015 | Inspection | Contains instruments to geo-locate | Pass by Section 2.6 |
| 016 | Inspection | Implemented autonomous navigation | Pass by Section 2.6 |
| 017 | Inspection | S and/or X band communication ability | Pass by Section 2.5 |
| 018 | Analysis<br>Inspection | Stability over 45° grade<br>Large wheels able to dig in soil | Pass by Section 2.9.2<br>Pass by Section 2.3 |
| 019 | Inspection | 10cm of suspension travel length | Pass by Sections 2.3, 2.9.3 |
| 020 | Analysis | No larger than 2m x 2m x 2m | Pass by Section 2.9.3 |

# K Finite Element Analysis

In order to integrate the research into the design of the rover to have it behave as intended, Finite Element Analysis (FEA), was used to go through multiple iterations of sub system designs to ensure the rover will preform to it's maximum ability. SolidWorks 3D Static simulations were used to generate the parts, with isolated sub-systems modeled in the same geometry of the CAD and UE5 renders. Aluminia was the material selected due to the close behavior of Al2219, models were loaded with respect to lunar gravity, and a fine mesh model was used.

## K.1 Fuel Tanks

Below depicts the main central fuel tank and support structures used to keep the fuel tank stable during launch and operations. The fuel tank was loaded with maximum pressure of 50bar and the only fixed features were the 3cm thick supports. The fuel tank had dimensions of 1.3m long, 0.3m diameter inner diameter, 1cm thick thickness, and 10cm long conic bulkheads to increase the durability. Under these conditions, it had a maximum deflection of 0.033mm, maximum von Mises stress of 98.2MPa, and a maximum Principle Stress of 84MPa, well within Al2219 tolerances for elastic deformation under maximum loading conditions. The original design featured the two outer supports, but testing revealed localized internal stress concentrations at these points, so a third support was added, producing a slightly higher stress but it was more uniform to decrease crack growth.

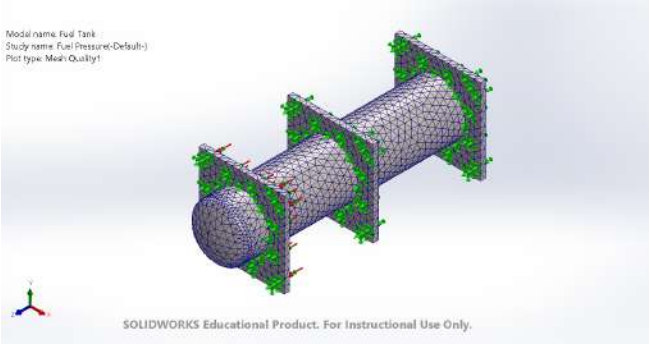


Figure 11: FEA: Main Fuel Tank Mesh

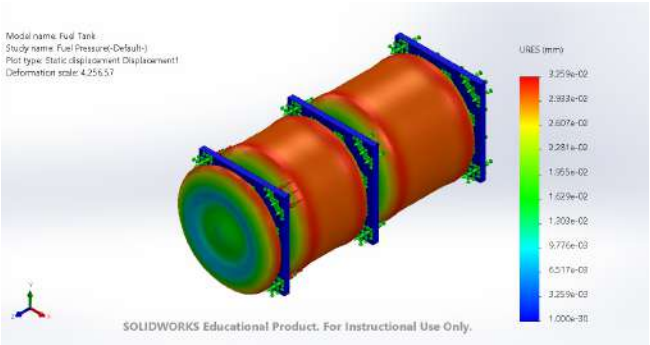


Figure 12: FEA: Main Fuel Tank Amplified Displacement


Figure 13: FEA: Main Fuel Tank von Mises Stress

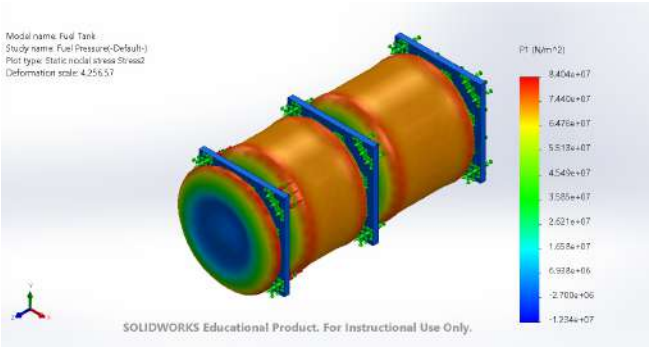


Figure 14: FEA: Main Fuel Tank Principle Stress

## K.2 Wheels

Below shows the planned elastic deformation of the wheel design. The deformation has been exaggerated by orders of magnitude in order to show stress concentrations, it will only deflect a maximum of 1cm at a load of 400N, 1.5x the load of a single wheel loading assuming uniform weight distribution and horizontal travel, to account for obstacles and different weight distributions depending on the orientation of LUNAR EMU. The wheels are 0.5m in diameter and 0.2m wide, with 4cm by 3mm paddles. Through multiple iterative designs to increase the elastic deformability of the wheel, the end result produced a maximum deflection of 3cm, creating a pseudo-non-pneumatic-lugged wheel.

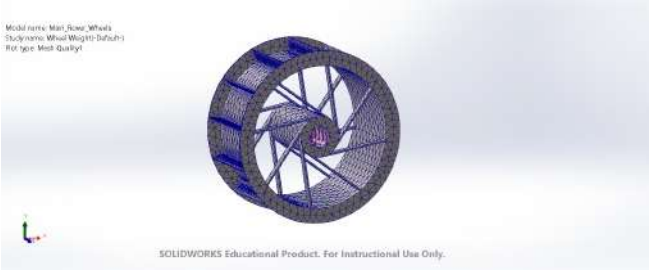


Figure 15: FEA: Wheel Mesh

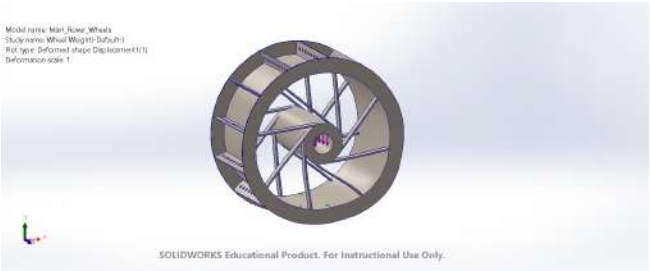


Figure 16: FEA: Wheel Displacement


Figure 17: FEA: Amplified Wheel Displacement


Figure 18: FEA: Wheel Strain

## K.3 Chassis

### K.3.1 Launch Durability

There is no publicly available information of the maximum launch acceleration of the SpaceX Falcon 9 Heavy, so a maximum of 9 g's of acceleration was assumed. Utilizing this assumption, the rover chassis was analyzed to determin the maximum stress and deflection. Under nominal launch conditions, there is a maximum deflection of 0.081mm and maximum von Mises stress of 30.4MPa, all within the elastic deformation zone of Al2219.

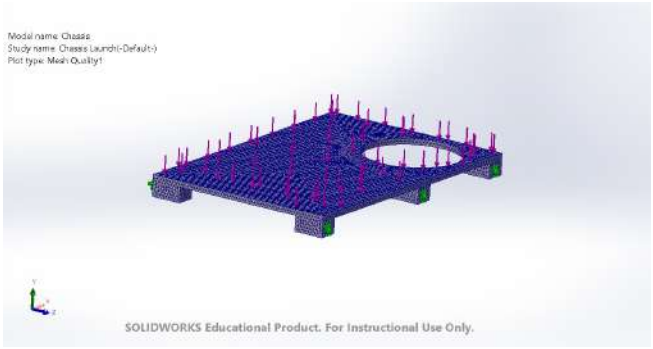


Figure 19: FEA: Chassis Launch Mesh

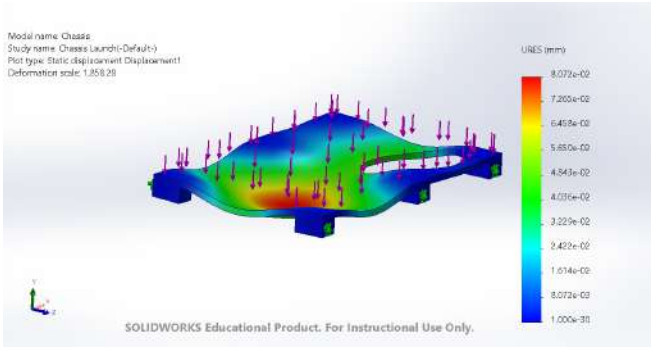


Figure 20: FEA: Chassis Launch Amplified Displacement

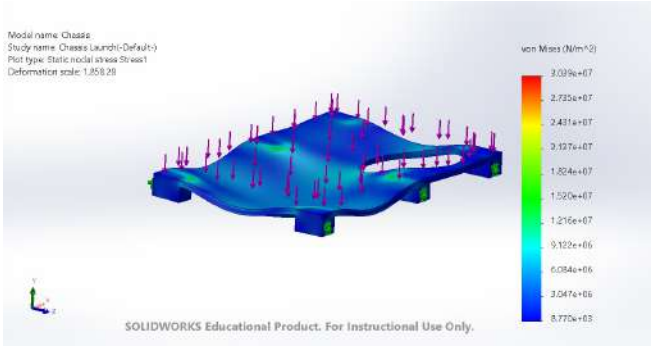


Figure 21: FEA: Chassis Launch von Misses Stress

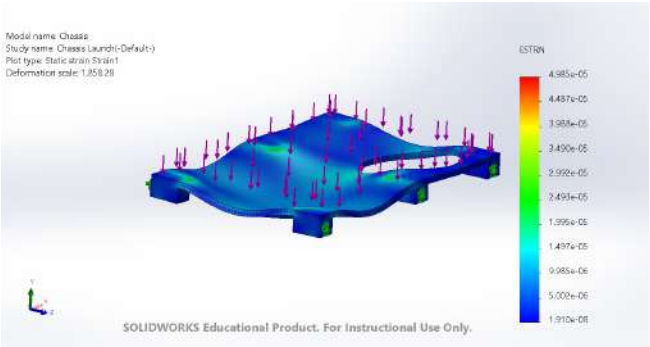


Figure 22: FEA: Chassis Launch Strain

### K.3.2 Lunar Operations

Utilizing the lunar gravity of 1.6 $\frac{m}{s^2}$, a uniform weight distribution was applied to the chassis, with a FOS of 2. It will have a maximum deflection of 0.0039mm and maximum von Mises stress of 1.4MPa, once more within the elastic deformation zone of Al2219.

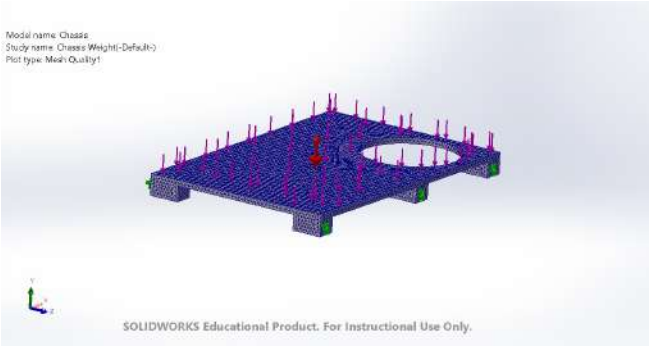


Figure 23: FEA: Chassis Lunar Operations Mesh

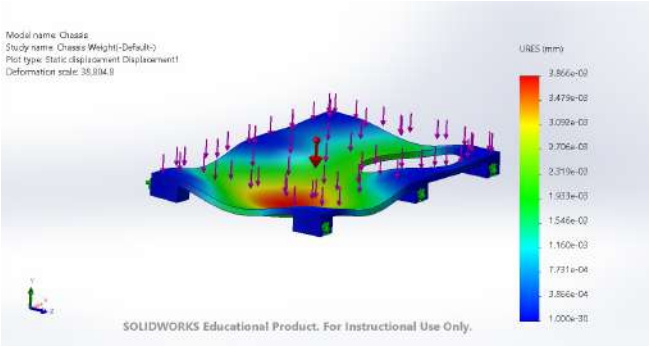


Figure 24: FEA: Chassis Lunar Operations Amplified Displacement

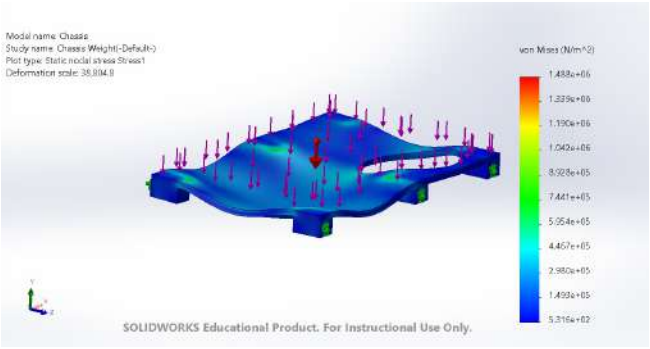


Figure 25: FEA: Chassis Lunar Operations von Mises Stress

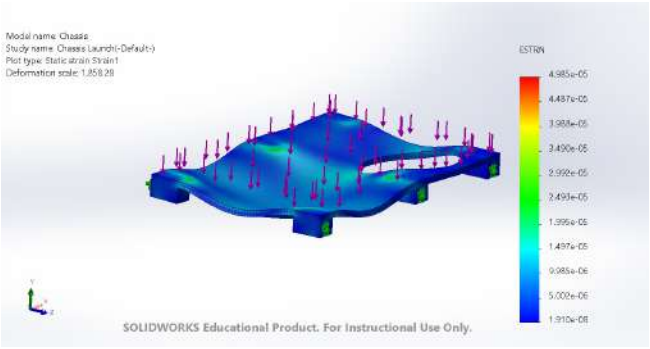


Figure 26: FEA: Chassis Lunar Operations Strain

## K.4 Torsional Bar Suspension

A moment of 255 Nm and shear force of 500N was applied to one end of a torsional bar, about double what the expected moment and force will be when the torsional bar is horizontal, simulating the worst circumstance with a FOS of 2. Utilizing the 3mm thick torsional bar, it has a natural deflection of 1.92mm, with a maximum von Mises Stress of 302.6 MPa. Although the stress will be high in the torsional bar, it is still about a third of the maximum yield stress at double the maximum loading conditions which will be enough to satisfy an enviorment LUNAR EMU will be in.


Figure 27: FEA: Torsional Bar Mesh

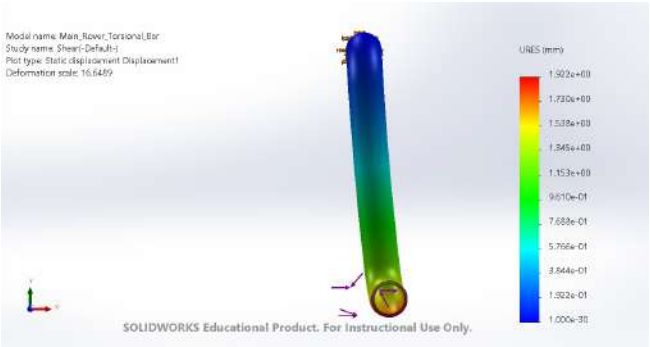


Figure 28: FEA: Torsional Amplified Displacement

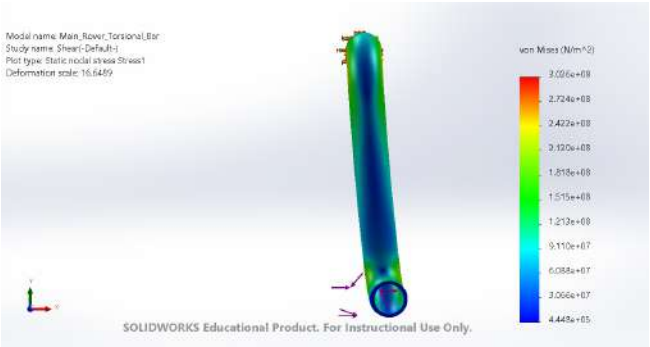


Figure 29: FEA: Torsional Bar von Mises Stress

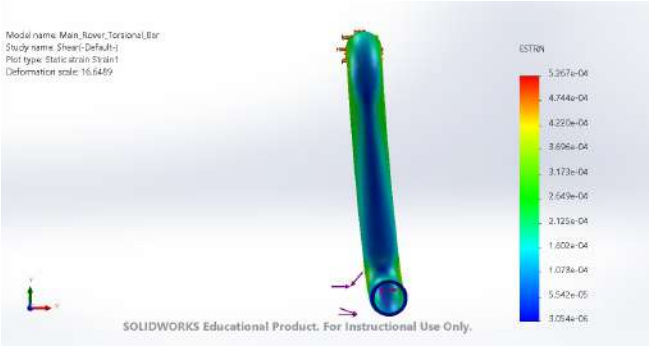


Figure 30: FEA: Torsional Bar Strain

# L Cost Estimates

| Subsystem | Item | Quantity | Unit Cost | Item Cost | Ref |
|---|---|---|---|---|---|
| Power | Hydrogen Engine | 1 | $50,595.00 | $50,595.00 | [74] |
| | H2 Fuel [0.717 kg] | 0.717 | $5.00 | $3.59 | [75] |
| | O2 Fuel [5.568 kg] | 5.568 | $12.75 | $70.99 | [76] |
| Thermal | Copper Piping [5m] | 5 | $7.22 | $36.12 | [77] |
| Scientific | 1 Visible Light Camera | 1 | $1,099.99 | $1,099.99 | [78] |
| | 1 NIR Camera | 1 | $2,689.00 | $2,689.00 | [79] |
| | 1 SWIR Camera | 1 | $966.00 | $966.00 | [80] |
| | 1 Night Vision Camera | 1 | $2,595.00 | $2,595.00 | [81] |
| | Curosity Rover SAM Unit | 1 | $31,200,000.00 | $31,200,000.00 | [82] |
| | 1m Drill | 1 | $1,499.00 | $1,499.00 | [83] |
| | 12 Fleet Seismometers | 12 | $6,048.00 | $72,576.00 | [84] |
| Mini Rover | 1 Night Vision Camera | 1 | $2,595.00 | $2,595.00 | [81] |
| | 1 NIR Camera | 1 | $2,689.00 | $2,689.00 | [79] |
| | High Density LiPo Batteries | 2 | $729.99 | $1,459.98 | [85] |
| COMM/NAV | X-band antenna | 1 | $4,630.00 | $4,630.00 | [86] |
| Wheels | Wheels [x8] | 8 | $140 | $1,120.00 | [87] |
| Suspension | Torsional Bars [x8] | 8 | $105.08 | $840.64 | [88] |
| Dust Mitigation | N2 [23L] | 23 | $2.00 | $46.00 | [89] |
| Rover Body | Aluminum Alloy 2219 | 9 | $6,073.54 | $54,661.85 | [90] |
| Launch | SpaceX Heavy | 1 | $150,000,000.00 | $150,000,000.00 | [91] |
| Sky Crane | Sky Crane | 1 | $31,200,000.00 | $31,200,000.00 | [81] |
| - | - | - | **Total** | **$212,600,126.56** | - |

# M Development and Testing Standards

Adhering to NASA's unmanned spaceflight standards, the following have been identified in the production and testing of LUNAR EMU [68].

NASA-HDBK-1005: NASA Space Mission Architecture Framework (SMAF) Handbook for Uncrewed Space Missions

NASA-HDBK-2203: NASA Software Engineering Handbook

NASA-HDBK-4001: Electrical Grounding Architecture for Unmanned Spacecraft

NASA-HDBK-4002: Mitigating In-Space Charging Effects-A Guideline

NASA-HDBK-4008: Programmable Logic Devices (PLD) Handbook

NASA-HDBK-4009: Space Telecommunications Radio Systems (STRS) Architecture Standard Rationale

NASA-HDBK-5010: Fracture Control Implementation Handbook for Payloads, Experiments, and Similar Hardware

NASA-HDBK-7010: Direct Field Acoustic Testing (DFAT)

NASA-HDBK-8739.19-2: Measuring and Test Equipment Specifications, NASA Measurement Quality Assurance Handbook - ANNEX 2

NASA-HDBK-8739.19-3: Measurement Uncertainty Analysis Principles and Methods, NASA Measurement Quality Assurance Handbook - ANNEX 3

NASA-HDBK-8739.19-4: Estimation and Evaluation of Measurement Decision Risk, NASA Measurement Quality Assurance Handbook - ANNEX 4

NASA-STD-1008: Classifications and Requirements for Testing Systems and Hardware to be Exposed to Dust in Planetary Environments

NASA-STD-4003: Electrical Bonding for NASA Launch Vehicles, Spacecraft, Payloads, and Flight Equipment

NASA-STD-5001: Structural Design and Test Factors of Safety for Spaceflight Hardware

NASA-STD-5006: General Welding Requirements for Aerospace Materials

NASA-STD-5009: Nondestructive Evaluation Requirements for Fracture Critical Metallic Components

NASA-STD-5017: Design and Development Requirements for Mechanisms

NASA-STD-5019: Fracture Control Requirements for Spaceflight Hardware

NASA-STD-5020: Requirements for Threaded Fastening Systems in Spaceflight Hardware

NASA-STD-7002: Payload Test Requirements

NASA-STD-7009: Standard for Models and Simulations

NASA-STD-7012: Leak Test Requirements

NASA-STD-8719.17: NASA Standard for Ground-Based Pressure Vessels and Pressurized Systems (PVS)

NASA-STD-8719.27: Implementing Planetary Protection Requirements for Space Flight

NASA-STD-8739.10: Electrical, Electronic, and Electromechanical (EEE) Parts Assurance Standard

Due to the LUNAR EMU being an unmanned rover in a high static environment, containing pressurized fuel tanks on a gravitational body, and carrying scientific payloads, these standards are applicable to the design architecture. They have been implemented where necessary in the LUNAR EMU design, such as utilizing cylindrical fuel tanks with dome bulkheads to help adhere to standard NASA-STD-7012: Leak Test Requirements, MBSE being implemented to fulfill NASA-STD-7009: Standard for Models and Simulations, and high factors of safety for NASA-STD-5001: Structural Design and Test Factors of Safety for Spaceflight Hardware.